UNCLASSIFIED

AD NUMBER

AD866743

LIMITATION CHANGES

TO:

Approved for public release; distribution is unlimited.

FROM:

Distribution authorized to U.S. Gov't. agencies and their contractors; Critical Technology; MAR 1970. Other requests shall be referred to Air Force Technical Application Center, VELA Seismological Cetner, Washington, DC 20333. This document contains export-controlled technical data.

AUTHORITY

usaf ltr, 25 jan 1972

THIS PAGE IS UNCLASSIFIED

AD 866743

ANALYSIS OF STRAIN SEISMOGRAPH DATA

6 March 1970

Prepared For

AIR FORCE TECHNICAL APPLICATIONS CENTER
Washington, D. C.

By

J. R. Woolson

SEISMIC DATA LABORATORY

Under

Project VELA UNIFORM

Sponsored By

ADVANCED RESEARCH PROJECTS AGENCY
Nuclear Monitoring Research Office

DDC
RECEIVED
MAR 30 1970
C

Reproduced by the
CLEARINGHOUSE
for Federal Scientific & Technical
Information Springfield Va. 22151

THIS DOCUMENT IS SUBJECT TO SPECIAL EXPORT CONTROLS AND EACH TRANSMITTAL TO FOREIGN GOVERNMENTS OR FOREIGN NATIONALS MAY BE MADE ONLY WITH PRIOR APPROVAL OF CHIEF, AFTAC. Alexandria VA 22313

BEST
AVAILABLE COPY

ANALYSIS OF STRAIN SEISMOGRAPH DATA

SEISMIC DATA LABORATORY REPORT NO. 250

AFTAC Project No.:	VELA T/9706
Project Title:	Seismic Data Laboratory
ARPA Order No.:	624
ARPA Program Code No.:	9F10
Name of Contractor:	TELEDYNE INDUSTRIES, INC.
Contract No.:	F33657-69-C-0913-PZ01
Date of Contract:	2 March 1969
Amount of Contract:	$ 2,000,000
Contract Expiration Date:	1 March 1970
Project Manager:	Royal A. Hartenberger (703) 836-7647

P. O. Box 334, Alexandria, Virginia

AVAILABILITY

This document is subject to special export controls and each transmittal to foreign governments or foreign nationals may be made only with prior approval of Chief, AFTAC.

This research was supported by the Advanced Research Projects Agency, Nuclear Monitoring Research Office, under Project VELA-UNIFORM and accomplished under technical direction of the Air Force Technical Applications Center under Contract F33657-69-C-0913-PZ01.

Neither the Advanced Research Projects Agency nor the Air Force Technical Applications Center will be responsible for information contained herein which may have been supplied by other organizations or contractors, and this document is subject to later revision as may be necessary.

ABSTRACT

Noise power on the short period pendulum and strain instruments has been compared at WMO and HNME. In the response band of the short period instruments, there are approximately four decades of relative power at HNME, and two decades at WMO. In one case analyzed the noise power at HNME is about 2½ times the noise power at WMO at 1 Hz.

Coherence was estimated as a measure of the existence of a linear transfer function between the vertical strain and the vertical pendulum. At HNME there exists a well-defined linear transfer function in the band 0.1 to 0.6 Hz. The low coherence at higher frequencies at HNME and throughout the 0.1 to 3.0 Hz band at WMO rule out the possibility of a linear transfer function between the vertical strain and vertical pendulum.

Multiple coherence, and rotation of the horizontal short period seismograms were used to infer the existence of unidirectional noise components. At HNME about 80 percent of the noise power is unidirectional in the 0.3 to 0.4 Hz band. At WMO the noise field has no apparent single preferred direction. Preliminary work on rotation of the horizontal strain instruments at WMO is presented. The technique uses a third horizontal instrument to establish the shear component of strain.

Examples of detailed analysis to establish wavetype using the vertical strain, together with the vertical pendulum and horizontal pendulum instruments are included.

TABLE OF CONTENTS

	Page No.
ABSTRACT	
INTRODUCTION	1
TECHNICAL DISCUSSION	2
Site geology	2
Noise power comparison	2
Squared coherence comparison	3
Estimation of the transfer function	5
Noise source direction	8
Squared Multiple Coherence	8
Horizontal pendulum rotation	9
WMO strain seismogram rotation	10
Squared coherence of short samples at WMO	11
Noise at HNME at 2.6 Hz	12
Noise at HNME 0.5 to 1.2 Hz	13
CONCLUSIONS AND CURRENT WORK	15
REFERENCES	16
APPENDIX I	
Data Used in Preparation of Report	

LIST OF FIGURES

Figure Title	Figure No.
WMO - Power Spectrum Vertical Pendulum.	1
HNME - Power Spectrum Vertical Pendulum.	2
HNME - Power Spectrum Vertical Pendulum.	3
WMO - Power Spectrum Vertical Pendulum.	4
WMO - Power Spectrum Vertical Strain.	5
HNME - Power Spectrum Vertical Pendulum.	6
HNME - Vertical Strain.	7
HNME - Squared Coherence.	8
WMO - Squared Coherence - Vertical Strain to Vertical Pendulum.	9
HNME - Phase Difference Vertical Strain-Vertical Pendulum.	10
Squared Multiple Coherence - Horizontal Pendulums to Vertical Pendulums.	11
HNME - Squared Multiple Coherence.	12
HNME - Squared Multiple Coherence.	13
Squared Multiple Coherence - Horizontal Pendulums to Vertical Pendulums.	14
HNME - Pendulum Rotation.	15
HNME - Pendulum Rotation Filtered 0.1 to 0.5 Hz.	16
HNME - Pendulum Rotation Filtered 0.5 to 1.2 Hz.	17
HNME - Pendulum Rotation Filtered 1.2 to 2.4 Hz.	18
WMO - Pendulum Rotation.	19
WMO - Pendulum Rotation Filtered 0.01 to 0.5 Hz.	20
WMO - Pendulum Rotation Filtered 0.5 to 1.6 Hz.	21

LIST OF FIGURES (Cont'd.)

Figure Title	Figure No.
WMO - Pendulum Rotation Filtered 1.6 to 2.4 Hz.	22
WMO - Strain Rotation.	23
WMO - Strain Rotation Filtered 0.01 to 0.5 Hz.	24
WMO - Strain Rotation Filtered 0.5 to 1.6 Hz.	25
WMO - Strain Rotation Filtered 1.6 to 2.4 Hz.	26
WMO - Squared Coherence - Vertical Strain to Vertical Pendulum.	27
WMO - Squared Coherence - Vertical Strain to Vertical Pendulum.	28
WMO - Detail of Coherent Noise.	29
HNME - Relative Power Spectra-Vertical Strain and Vertical Pendulum.	30
P-Wave Phase Comparison.	31
HNME - Phase Difference Vertical Strain-Vertical Pendulum.	32
HNME - Pendulum Rotation Filtered 1.3 Hz to 5.2 Hz.	33
HNME - Phase Comparison - 2.6 Hz.	34
HNME - Phase Comparison (0.5-1.2 Hz).	35
HNME - Phase Comparison (0.5-1.2 Hz).	36
HNME - Phase Comparison (0.5-1.2 Hz).	37

LIST OF TABLES

HNME Noise Power Comparison	Table I

INTRODUCTION

Benioff (1935) described a linear strain seismograph and summarized early work on earth strain; Benioff and Gutenburg (1952) compared the response of strain and pendulum seismographs to earthquake generated Rayleigh waves. Romney (1964) and Benioff (1962) from somewhat different aspects considered the response to surface waves and P-waves, of combinations of pendulum and strain seismographs. Smith (1966) applied strain seismographs to analysis of free oscillations of the earth excited by large earthquakes. Shopland (1966) described the strain installation of WMO. Press (1965) exhibited two examples of apparent permanent changes in the strain associated with earthquake events. Gupta (1966) published a theoretical study of strain to pendulum seismograph response ratios.

The above cited papers taken together with a number of reports published by Teledyne Industries, Geotech Division, constitute the background for this study, which attempts to describe the noise field at several sites and to develop methods of signal enhancement using strain seismometers.

Data from two sites are examined in this report. These are WMO (Wichita Mountains Observatory) and HNME (The Long Range Seismic Measurement station at Houlton, Maine). Both sites have long and short period pendulum instruments; HNME has a vertical strain instrument; and WMO has orthogonal strain instruments. The data used in preparation of this report is listed in Appendix I.

TECHNICAL DISCUSSION

Site geology

WMO is located in the Wichita Mountains of West Central Oklahoma. The Wichita Mountains are the outcropping portion of a major granitic thrust from the south. The Anadarko basin north of the Wichitas is asymmetric; its deepest area being near the mountains. The north flank of the Wichitas exhibits evidence of overthrusting and complex folding.

HNME is located in east central Maine near the New Brunswick border. The outcropping rocks are Silurian, and consist of interbedded marine sediments, tuffs, and lavas. The general region is characterized by complex intrusions and folding. The youngest rocks in the region are probably Paleozoic. It is approximately 150 km from the Atlantic coast line.

Noise power comparison

Figures 1 and 2 compare relative noise power spectra as recorded on the vertical short period pendulum instruments at WMO and HNME. Calibration of Figures 1 and 2 shows the noise level to be 0.52 $(m\mu/sec)^2/Hz$ at 1.0 Hz at WMO and 1.29 $(m\mu/sec)^2/Hz$ at 1.0 Hz at HNME. The noise at WMO includes about two orders of magnitude of relative power; at HNME it covers about four orders of magnitude. These plots have not been adjusted for system response. Both pendulum instruments show a narrow peak in the noise at higher frequencies, 2.6 cps at HNME and 2.0 cps at WMO. Figure 3 is noise power at HNME, with less smoothing, included to illustrate better the noise peak at 2.6 cps. These

plots of short period power illustrate the noise field in which the strain instruments have been installed.

Figures 4 and 5 are comparable plots of seismic noise as recorded by the vertical strain and vertical pendulum at WMO. The higher relative power of the 2.0 cps noise on the pendulum as compared with the strain instrument is typical of a number of samples observed. This is consistent with the hypothesis that the noise is nearly vertical P waves which are not picked up on vertical strain instrument. This sample also contains a peak in the noise at 0.95 cps that has higher relative power on the pendulum instrument.

Approximate system noise level on the power spectra plots has been determined by observing the level at which the noise is white in the 5.0 to 10.0 Hz region; the assumption being that system noise is white throughout the range of frequencies analyzed.

Figures 6 and 7 compare the vertical pendulum and vertical strain at HNME. These plots show the increase in percentage variation of power from 0.4 Hz to 3.5 Hz and also show the greater relative response of the pendulum instrument to the 2.6 Hz noise. The energy at this frequency will be examined in some detail in a later section of this report.

Squared coherence comparison

Figures 8 and 9 are plots of the squared coherence between the vertical strain and vertical pendulum at HNME and WMO. These are typical of a number of samples of varying length and varying amounts of smoothing that were obtained.

The squared coherence is defined by

$$\kappa_{12}^2(f) = \frac{\alpha_{12}^2(f)}{\Gamma_{11}(f)\ \Gamma_{22}\ f)}$$

in which α_{12}^2 is the sum of the squares of the cospectrum and the quadspectrum between the two noise processes, and $\Gamma_{11}(f)$ and $\Gamma_{22}(f)$ are the power spectra of the two processes, see Jenkins and Watts (1968) p. 352.

At HNME the squared coherence between the vertical strain and vertical pendulum is greater than 0.9 between 0.15 and 0.4 Hz, and greater than 0.7 out to 0.6 Hz. The HNME plot (Figure 8) is interpreted to mean that there exists a well-defined linear transfer function between the vertical strain, and vertical pendulum in the 0.15 to 0.6 Hz band; the decrease in squared coherence for frequencies >0.6 Hz can be caused either by added random noise on one of the instruments or by a mixture of two or more linear processes.

Each of the plots of coherence, and later of multiple coherence, includes a horizontal dashed line, which marks the 95 percent confidence limit that the true squared coherence is zero. This limit is obtained by assuming two independent time series and noting that the estimated squared coherence approximately follows a Fisher F-distribution. Substitution of the number of degrees of freedom and use of tabulated data produces a quadratic, which may be solved for the 95 percent confidence limit. Experience using these results on a number of samples of varying lengths with a variety of degrees of freedom, indicates the validity of the 95 percent confidence limit. This can be seen, for example, in Figure 8. (Jenkins and Watts (1968) p. 433).

It is also possible to compute confidence limits of the

observed value of the squared coherence. The essential elements of this procedure are the transformation of the coherence using a Fisher z-transformation.

$$Y_{12}(f) = \text{arctanh } [|\overline{K}_{12}|]$$

Y_{12} is approximately normally distributed. (Jenkins and Watts, 1968, p. 379-380; Cramer, 1946, p. 398-401.) Bendat and Piersoll (1966, p. 214) use a similar formula to establish an estimated value of squared coherence. For $\overline{K}_{12}^2 = 0.9$ and 32 degrees of freedom, the 95 percent confidence limits are

$$0.83 \leq K_{12}^2 \leq 0.94$$

which fits the observed variation of Figure 8.

Figure 9 is a typical plot of the observed squared coherence at WMO. The 95 percent confidence limit is marked on this plot for 0.155 and 0.31 Hz. There can be no well-defined linear transformation between the vertical strain and vertical pendulum at WMO. Inspection of the raw data, however, reveal short segments of 5.0 to 10.0 seconds duration during which a linear transformation exists. A sample of this sort will be examined in detail in a following section.

Estimation of the transfer function

In order to obtain an estimate of the linear relation between the vertical strain and vertical pendulum a model of the form

$$X_2(t) = \int_o^\infty h(u)\, X_1\,(t-u)\, du + Z(t)$$

is taken. Following Jenkins and Watts (1968, p. 351), if the cross covariance of the output is taken and then Fourier transformed

$$H(f) = \frac{\Gamma_{12}(f)}{\Gamma_{11}(f)}$$

in which $\Gamma_{12}(f)$ is the complex cross spectrum of the output and input and $\Gamma_{11}(t)$ is the input autospectrum.

Writing

$$H(f) = G(f)e^{+i\phi(f)} = \frac{\Lambda_{12}(f) - i\Psi_{12}(f)}{\Gamma_{11}(f)}$$

in which

$$G(f) = [\Lambda_{12}^2(f) + \Psi_{12}^2(f)]^{1/2}/\Gamma_{11}(f) = \alpha_{12}(f)/\Gamma_{11}(f)$$

which defines $\alpha_{12}(f)$, and

$$\Phi(f) = \arctan - \frac{\Psi_{12}(f)}{\Lambda_{12}(f)}$$

The squared coherency is defined as

$$\kappa_{12}^2 = \frac{\alpha_{12}^2(f)}{\Gamma_{11}(f)\Gamma_{22}(f)}$$

then

$$H(f) = \kappa_{12}(f)\left[\frac{\Gamma_{22}(f)}{\Gamma_{11}(f)}\right]^{1/2} e^{i\phi(f)}$$

In comparing HNME and WMO, two cases occur. Figure 10 is plot of $\phi(f)$ for several examples of HNME data. For $f \leq 1.0$ Hz, $\phi(f) \simeq \pi/2$; thus

$$H(f) \simeq K_{12}(f)\left[\frac{\Gamma_{22}}{\Gamma_{11}}\right]^{\frac{1}{2}}(-i)$$

At WMO a number of computations, of which Figure 9 is an example, show that κ_{12} is less than the 95 percent confidence limits that the squared coherence is zero. That is at WMO

$$H(f) \simeq 0$$

In the model assumed this means that

$$X_2(t) = Z(t)$$

that is the vertical pendulum looks like noise when compared with the vertical strain.

Returning to HNME, the values in

$$H(f) = -jK_{12}(f)\left[\frac{\Gamma_{22}}{\Gamma_{11}}\right]^{\frac{1}{2}}$$

are given in Table 1, at 0.31 Hz for a sequence of 512 point samples 1000 pts (50 seconds) apart.

Thus for any given moment one can expect any fixed linear transfer function to fail to cancel some 7 percent of the noise amplitude and in extreme cases as much as 10 percent of the noise at 0.312 Hz. It is assumed that the vertical strain output is phase shifted 90° and then subtracted from the vertical pendulum. This is another way of looking at the fact that the

coherence is not 100 percent, i.e., some of the power on the vertical pendulum cannot be predicted by the vertical strain.

Noise source direction

Squared Multiple Coherence

Two techniques are used to analyze the noise source direction at WMO and HNME. They are squared multiple coherence, and rotation of the horizontal instruments.

The squared multiple coherence is defined as

$$\kappa^2_{(q+1)123\ldots q} = 1 - \frac{|\hat{\Gamma}_{(q+1)(q+1)}(f)|}{\Gamma_{(q+1)(q+1)}(f)\,|\hat{\Gamma}_{qq}(f)|}$$

where $\hat{\Gamma}_{qq}$ is the spectral matrix of the stochastic process. For the case of two inputs (q=2) and one output as used in this report, the above formulation becomes

$$\kappa^2_{312} = 1 - \frac{\begin{vmatrix} \Gamma_{11} & \Gamma_{12} & \Gamma_{13} \\ \Gamma_{21} & \Gamma_{22} & \Gamma_{23} \\ \Gamma_{31} & \Gamma_{32} & \Gamma_{33} \end{vmatrix}}{\Gamma_{33} \begin{vmatrix} \Gamma_{11} & \Gamma_{12} \\ \Gamma_{21} & \Gamma_{22} \end{vmatrix}}$$

where, for example, Γ_{12} is the cross-spectrum between channels 1 and 2 and Γ_{11} is the autospectrum of channel 1. The squared multiple coherence measures the proportion of the output channel that can be predicted from the inputs (Jenkins and Watts, 1968, p. 487-488). As applied here, the horizontal instruments are used as inputs, and the vertical instrument is the output. If the squared multiple coherence is high, one would expect the noise to be unidirectional and therefore, to find a linear

transformation between the horizontal and vertical component of the noise. Low coherence can be caused either by multi-directional noise or by the absence of a time invariant linear transfer function between the horizontal and vertical components of the noise.

Figures 11 through 14 are examples of the squared multiple coherence as obtained at WMO and HNME. Typically, the squared multiple coherence has values near 0.8 at 0.3 Hz at HNME; at WMO the value is consistently below or near the 95 percent confidence limit that the true multiple coherence is different from zero. The high squared multiple coherence at 2.6 Hz at HNME appears to be a special case and will be examined in detail.

Horizontal pendulum rotation

If there exist short segments (5 to 10 seconds) of the noise that are unidirectional; then by rotation of the horizontal pendulums so that one component is aligned with the noise source direction and the other is perpendicular to it, the maximum amplitude should occur on one component and the minimum amplitude on the component at 90 degrees to the azimuth.

Figures 15 through 18 are examples of the horizontal pendulums at HNME rotated in 15 degrees steps starting from their installed azimuths. The sample chosen is the same as that used to obtain the squared multiple coherence of Figure 11. Clearly, if the noise has two or more source directions at the same time, this technique will not identify the direction. Figure 15 is the original rotated seismograms. Figures 16 through 18 are the rotated seismograms filtered as marked. On each of the filtered sets, segments of noise that appear to

be unidirectional are enclosed in a box. The seismograms filtered 0.1 to 0.5 Hz appear to have a predominance of noise from 3° or 183° (the technique does not allow one to distinguish sense). The 0.5 to 1.2 Hz band (Figure 16) has no apparent source direction, yet some scattered unidirectional segments occur. The band 1.2 to 2.4 Hz (Figure 17) shows that much of the 2.6 Hz energy has an azimuthal direction of 168° or 348°. This phenomenon will be examined in detail.

Figures 19 through 22 have the same format as Figures 15 through 18; the data is now from WMO. The same technique has been used to mark apparent unidirectional segments. The squared multiple coherence analysis at WMO indicated little if any unidirectional noise, and no dominant direction is apparent on the filtered seismogram. The data used is about the same as that for Figure 11.

WMO strain seismogram rotation

In order to rotate the strain seismograms it is necessary to use plane strain theory which implies that two of the principal strain axes are in the horizontal plane. It is also necessary to use a third strain seismometer to determine the shear component of strain. Jaeger (1962, p. 42) writes the rotated components of strain relative to the original components in the form

$$\varepsilon_x' = \varepsilon x \cos^2\theta + \gamma_{xy}\sin\theta\cos\theta + \varepsilon_y\sin^2\theta$$

$$\varepsilon_y' = \varepsilon_x \sin^2\theta - \gamma_{xy}\sin\theta\cos\theta + \varepsilon_y\cos^2\theta$$

In which ε_x, ε_y are the linear strain components and γ_{xy} is the shear component of the strain tensor, and θ is the angle through which the strain coordinates are rotated. Designating the north component of strain by SN, the east by SE and the northwest by SNW, the above equations becomes

$$\varepsilon_x' = SE\cos^2\theta + (SE+SN-2SNW)\sin\theta\cos\theta + SN\sin^2\theta$$

$$\varepsilon_y' = SE\sin^2\theta - (SE+SN-2SNW)\sin\theta\cos\theta + SN\cos^2\theta$$

The 45 degrees azimuthal difference between north and northwest gives this equation a particularly simple form.

Figures 23 through 26 are the result of applying the above formula to three of the horizontal strain components at WMO. Apparent unidirectional segments of data have been enclosed in rectangles. The analysis could not be repeated at HNME because of the absence of horizontal strain seismometers.

Squared coherence of short samples at WMO

Figures 27 and 28 are plots of the squared coherence between the vertical strain and vertical pendulum at WMO. The samples occur in two groups. Analysis of the squared coherence values and the sample intervals, show that the relatively high multiple coherence of one sample is caused by the coherence at the data between points 813 and 913. Figure 29 is a copy of the original seismogram on which the coherent segment has been marked. Examination of the rotated horizontal pendulums for this interval (Figure 20) shows that, the azimuthal direction of the coherent noise segment is 90 degrees (or 270 degrees), along the axis of the Wichita

Mountain thrust. The rotated strain seismograms do not exhibit a well-defined azimuthal direction. There exists a pulse from 105 degrees (or 285 degrees) which may be the same noise pulse as seen on the horizontal pendulum instruments. Figure 29 shows the 90 degrees phase shift expected for Rayleigh waves.

Noise at HNME at 2.6 Hz

At HNME for all samples there exists a peak in the noise spectra at 2.6 Hz. The noise has a sinusoidal appearance on most seismograms. A number of lines of evidence described below show that it is P-wave noise. The mechanism of its generation is left for later study.

Figure 30 is a detailed plot of the relative power on the vertical strain and vertical pendulum instruments at HNME. The higher peak of the pendulum relative to the strain is indicative of P-wave noise, since the vertical strain is less responsive to P-waves than the vertical pendulum (Romney, 1964). This same relative amplitude phenomena is also characteristic of the 2.0 Hz noise at WMO.

Figure 31 is the first motion of a well-defined earthquake event at HNME, which shows that PZ and SZ are in phase for P-waves. Figure 32 is the phase plots from four samples which show a phase difference of 360 degrees (or 0 degrees) at 2.6 Hz.

The squared multiple coherence of points 500-2547 HNME (Seis. 19028) has a value of 0.92 at 2.6 Hz (Figure 11). This means that for this sample the noise is nearly unidirectional. Other samples have lower squared multiple coherence indicating that the unidirectionality of this sample is not typical and therefore should not be ascribed to cultural noise originating

at a particular azimuth. Figure 33 are the rotated seismograms corresponding to the above described squared multiple coherence. The azimuth is well-defined at 168 degrees (or 348 degrees). The cosine azimuthal response of the horizontal instruments makes this value only approximate (say ± about 15°). The seismograms of Figure 33 have been band-pass filtered 1.3 to 5.2 Hz, 24 db/octave phaseless.

Figure 34 consists of samples from the 168 degree azimuth plot of Figure 33 compared with the vertical pendulum filtered 1.3 to 5.2 Hz. These samples show the general 0 degree phase differences expected from the above evidence.

Noise at HNME 0.5 to 1.2 Hz

At HNME the squared coherence vertical strain to vertical pendulum is commonly about 0.9 between 0.15 and 0.5 Hz, which means that there exists a well-defined linear transformation that can be used to cancel noise in this frequency band. Between 0.5 and 1.5 Hz the squared coherence decreases to values less than 0.2 which is below the 95 percent confidence limit that the linear transfer function in the frequency domain is not zero (Figure 8). Nonetheless the estimated phase angle remains relatively constant at about 270 degrees from 0.15 to 1.5 Hz. (Figure 32). This may reflect the existence of several different independent Rayleigh modes, each with a different transfer function amplitude but identical 270° phase shift.

Rotation of the horizontal pendulum instrument exhibits a few short segments of noise even between 0.5 and 1.5 Hz which appear to be unidirectional. In most cases the noise is not thus resolvable, meaning that the noise is arriving simultaneously at the site from two or more azimuths. Figures 35, 36, and 37 are examples of apparent unidirectional noise from Seismogram 19028 between points 500 and 2500. These data are also plotted

in Figure 16 while Figures 15 and 17 give the corresponding plots for the frequency bands 0.1 to 0.5 and 1.2 to 2.4 Hz. The criteria for a single direction noise is low noise level on the instrument at 90 degrees to the apparent source azimuth. The portion of noise analyzed has been band-pass filtered (0.5 to 1.2 Hz, 24 db/octave, phaseless).

Figure 35, the shaded pulse, shows a direction whose azimuth is 168 degrees (or 348 degrees). The vertical pendulum is 90 degrees out of phase, and the vertical strain is 180 degrees out of phase with the rotated horizontal seismogram as would be expected for Rayleigh waves.

Figure 36, the shaded pulse, illustrates a unidirectional noise pulse that is apparently not a Rayleigh wave. There should be a 0° or 180° phase difference between vertical strain and horizontal pendulum for Rayleigh waves. This noise pulse has a 90 degree phase difference. The fact that the vertical pendulum is 180 degrees out of phase with the rotated horizontal pendulum indicates a P or SV-wave. The 90 degree phase difference between the vertical strain and vertical pendulum also indicates a P or SV wave. If it is an SV-wave it may be shown that its angle of incidence is less than critical.

Figure 37 illustrates two pulses on the horiztonal instruments which seem to merge into a single pulse on the vertical instruments. The first portion (3 degree azimuth) has the characteristics of a Rayleigh wave. The 93 degree azimuth pulse is in phase on all three instruments. Preliminary identification is that this is an SV-wave whose angle of incidence is greater than the critical angle.

This brief examination of the noise field in the 0.5 to 1.2 Hz band suggests that the decreasing squared coherence above about 0.5 Hz is due to a mixture of wave types.

CONCLUSIONS AND CURRENT WORK

At HNME the evidence is clear that short period noise, 0.15 to 0.60 Hz, can be cancelled by a linear combination of the vertical strain and vertical pendulum. Over 80 percent of this noise can be shown to be unidirectional. Between 0.6 and 2.0 Hz, the coherence is low, indicating that no linear combination exists which will cancel the noise. This noise apparently comes from many directions. Despite this, the relative phase between the two instruments is stable at 90 degrees over the entire frequency band 0.1 to 2.0 Hz, indicating perhaps that some small component of the noise between 0.6 and 2.0 Hz is Rayleigh waves which may be cancelled out. An alternative hypothesis is that of energy in several different Rayleigh modes. At 2.6 Hz there is a well defined band of P-wave noise.

Further studies at HNME are concentrating on analysis of the several phases generated by an earthquake near Morocco, with a view to seeing how each of them is detected on the complete array of instruments.

WMO has no frequency band in which a well-defined transfer function exists or in which the noise is unidirectional. Further research will be pointed toward giving a physical explanation of why this is in order to establish criteria for the applicability of the strain system to a particular site. We plan to do this by examining earthquake phases which arrive at WMO from different azimuths traversing nearby geologic structures of greater or lesser complexity.

REFERENCES

Bendat, J.S. and A.G. Piersoll, 1966, Measurement and analysis of random data: John Wiley & sons.

Benioff, H., 1935, A linear strain seismograph, BSSA 25, p. 283-309.

Benioff, H., 1962, The characteristics of strain and pendulum seismograph combinations, Proceedings of the Colloquium on Detection of Underground Nuclear Explosions, p. 442-455.

Benioff, H. and B. Gutenburg, 1952, The response of strain and pendulum seismographs to surface waves, BSSA 43, p. 229-237.

Blayney, J.L. and R. Gilman, 1965, A portable strain meter with continuous interferometric calibration, BSSA 55, p. 955-970.

Cramer, H., 1946, Mathematical methods of statistics, Princeton University press.

Gupta, I.N., 1966, Response of a vertical strain seismometer to body waves, BSSA 56, p. 785-791.

Jaeger, J.C., 1962, Elasticity, fracture and flow, Methuen and Co., Ltd.

Jenkins, G.M. and D.G. Watts, 1968, Spectral analysis and its applications: Holden-Day.

Press, F., 1965, Displacements, strains and tilts at teleseismic distances, J. Geophys. Res., v. 70, p. 2395-2412.

Romney, C., 1964, Combinations of strain and pendulum seismographs for increasing the detectability of P, BSSA 54, p. 2165-2174.

Shopland, R.C., 1966, Shallow strain seismograph installation at the Wichita Mountain Seismological Observatory, BSSA 56, p. 337-360.

TABLE I

HNME Noise Power Comparison

Seis. 19028 @ 0.31 Hz

Points	PZ Power	SZ Power	$\frac{PZ}{SZ}^{\frac{1}{2}}$	K_{12}	Xi $K_{12}\frac{PZ}{SZ}^{\frac{1}{2}}$	$(X_i-\mu)^2$
500-1011	5.561×10^3	1.394×10^4	.632	.97	.613	.004761
1500-2011	6.282×10^3	1.267×10^4	.703	.97	.682	.000000
2500-3011	2.020×10^3	3.908×10^4	.717	.94	.675	.000049
3500-4011	8.027×10^3	1.473×10^4	.737	.97	.715	.001089
4500-5011	5.759×10^3	1.072×10^4	.731	.97	.710	.000784
5500-6011	8.915×10^3	1.495×10^4	.771	.98	.756	.005476
6500-7011	3.180×10^3	4.750×10^3	.820	.88	.723	.001681
7500-8011	5.139×10^3	1.245×10^4	.634	.97	.615	.004489
8500-9011	3.818×10^3	7.773×10^3	.702	.97	.681	.000001
9500-10,011	6.082×10^3	1.055×10^4	.772	.97	.750	.004624

Mean = μ = 0.682

σ^2 = 0.00255

σ/μ = 0.074

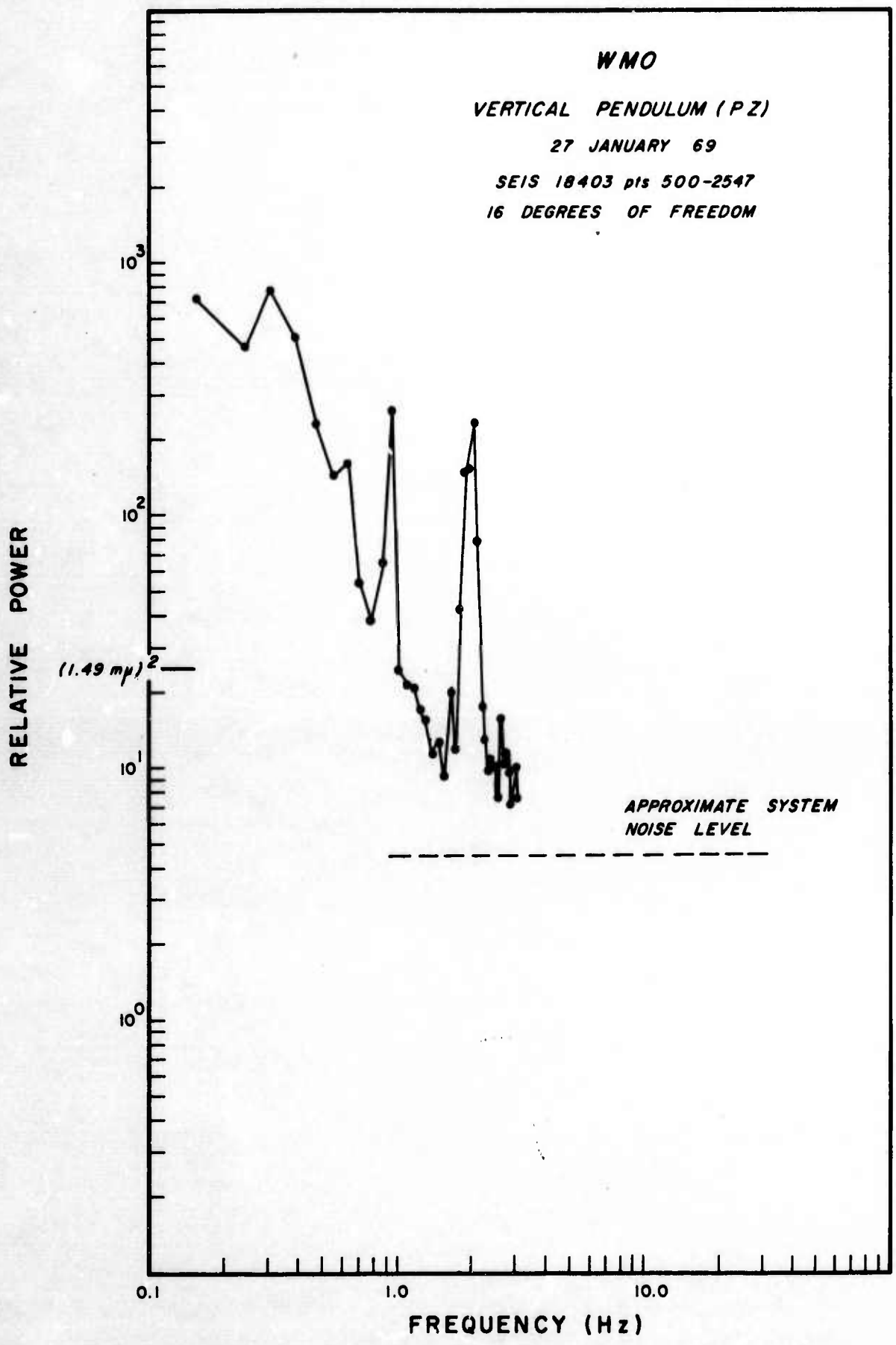

Figure 1. WMO - Power Spectrum Vertical Pendulum.

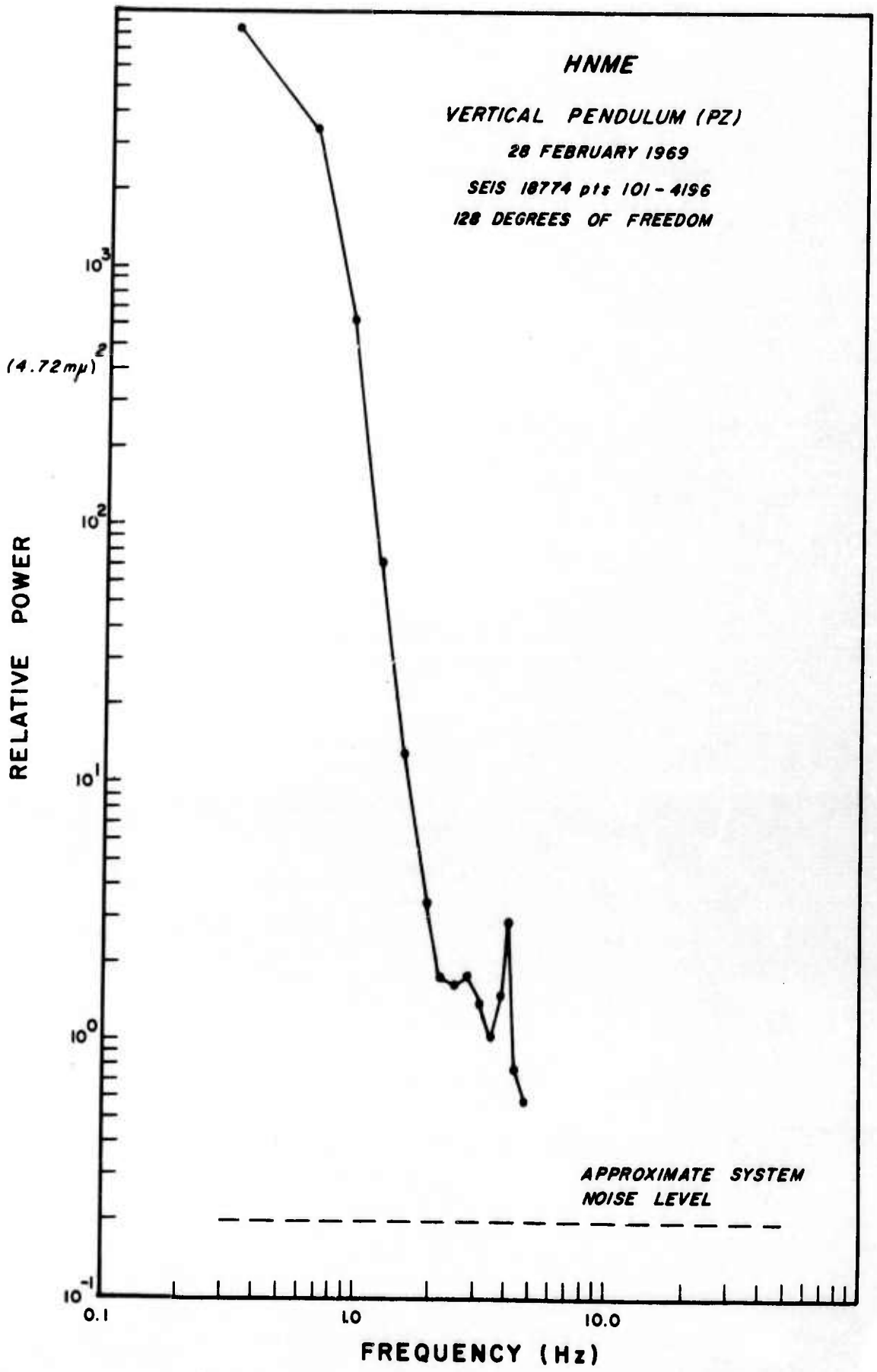

Figure 2. HNME - Power Spectrum Vertical Pendulum.

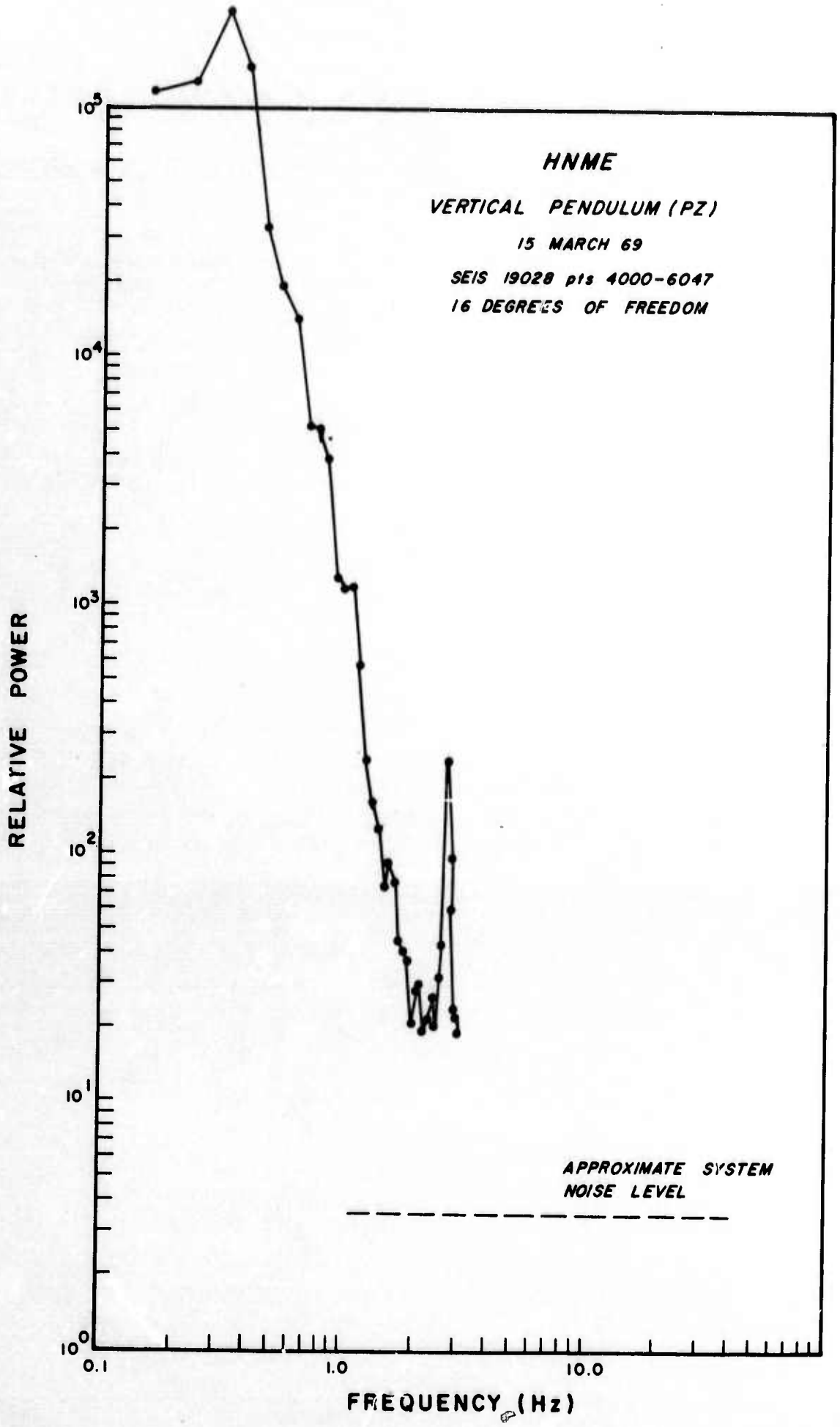

Figure 3. HNME - Power Spectrum Vertical Pendulum.

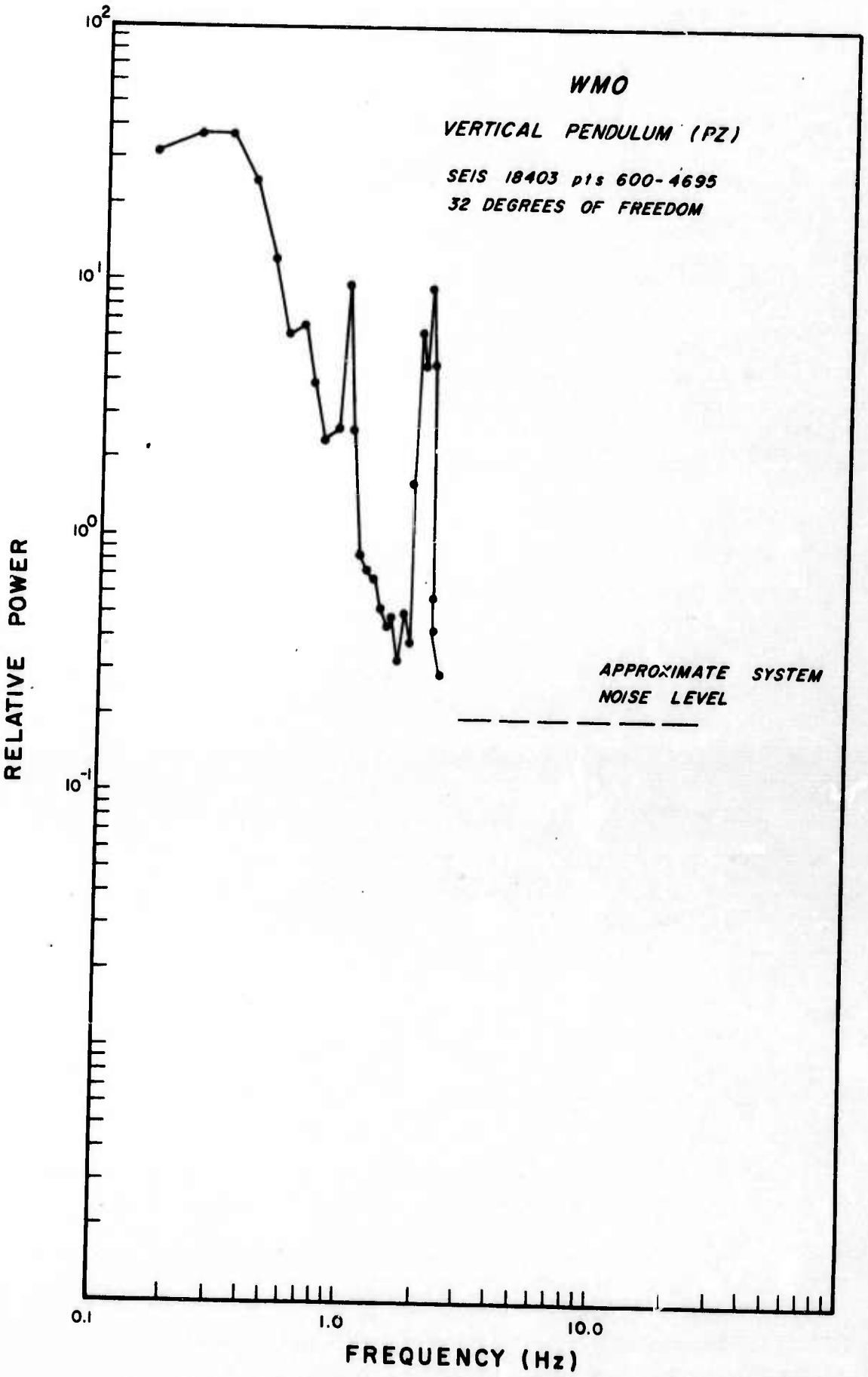

Figure 4. WMO - Power Spectrum Vertical Pendulum.

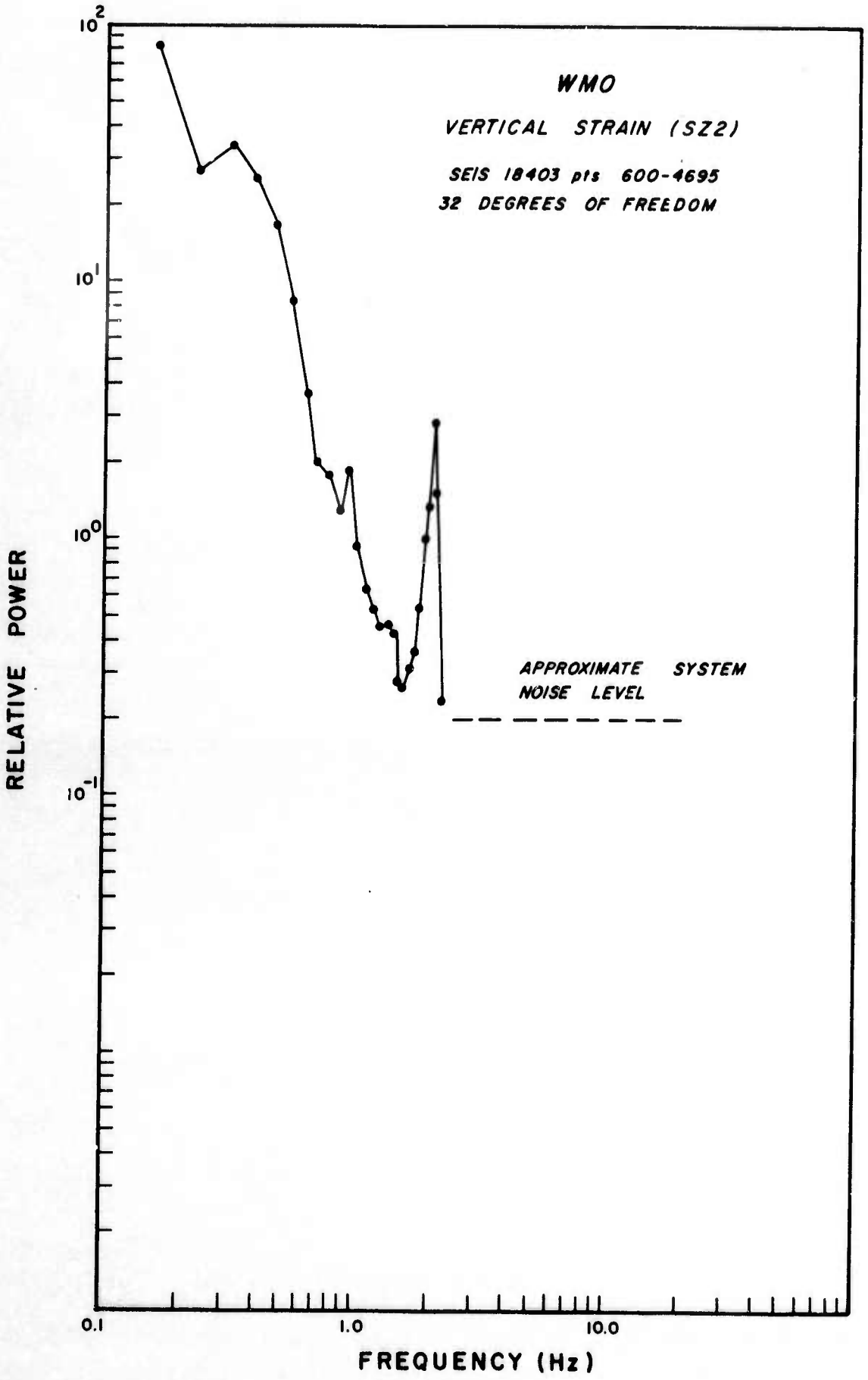

Figure 5. WMO - Power Spectrum Vertical Strain.

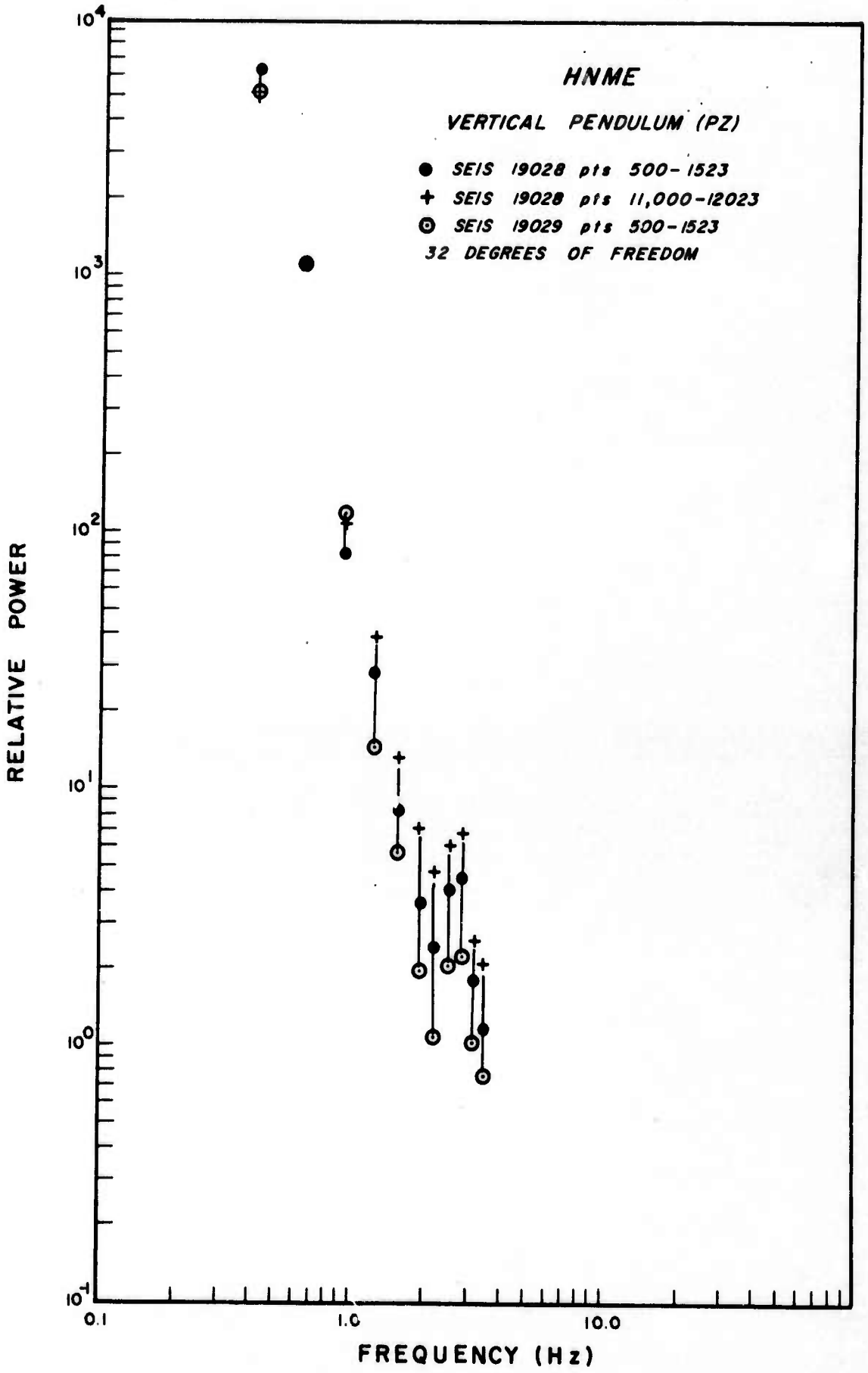

Figure 6. HNME - Power Spectrum Vertical Pendulum.

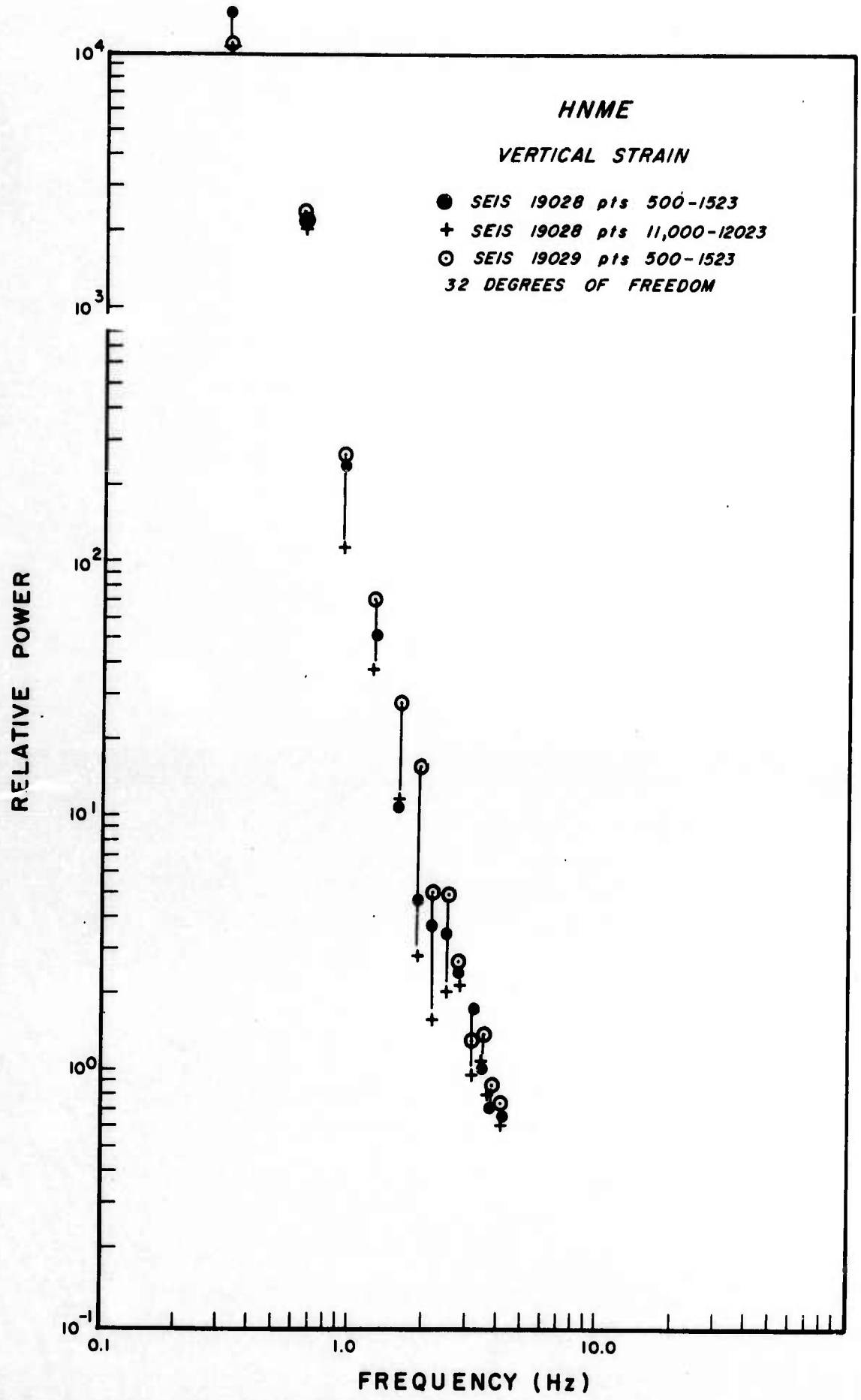

Figure 7. HNME - Vertical Strain.

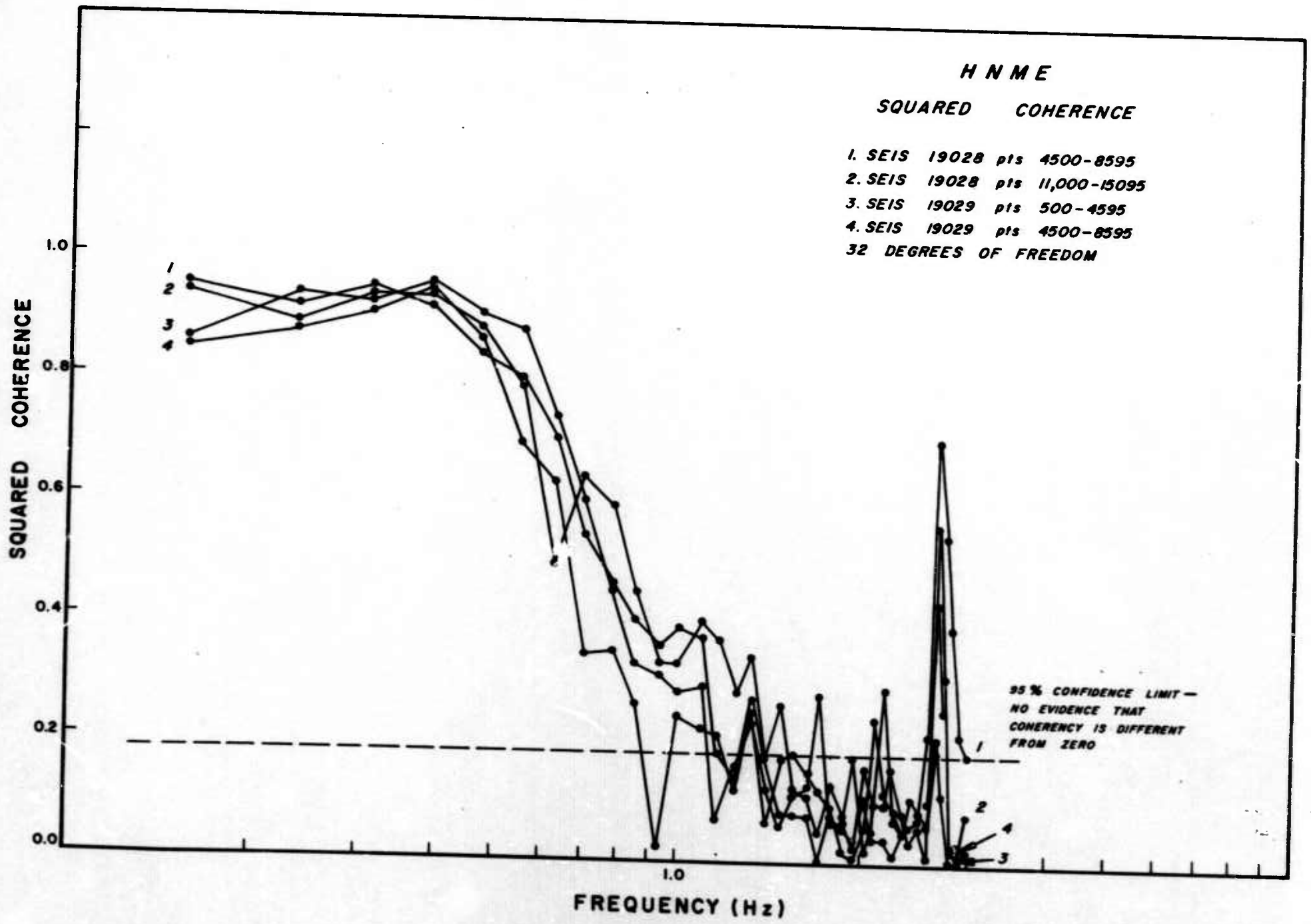

Figure 8. HNME - Squared Coherence.

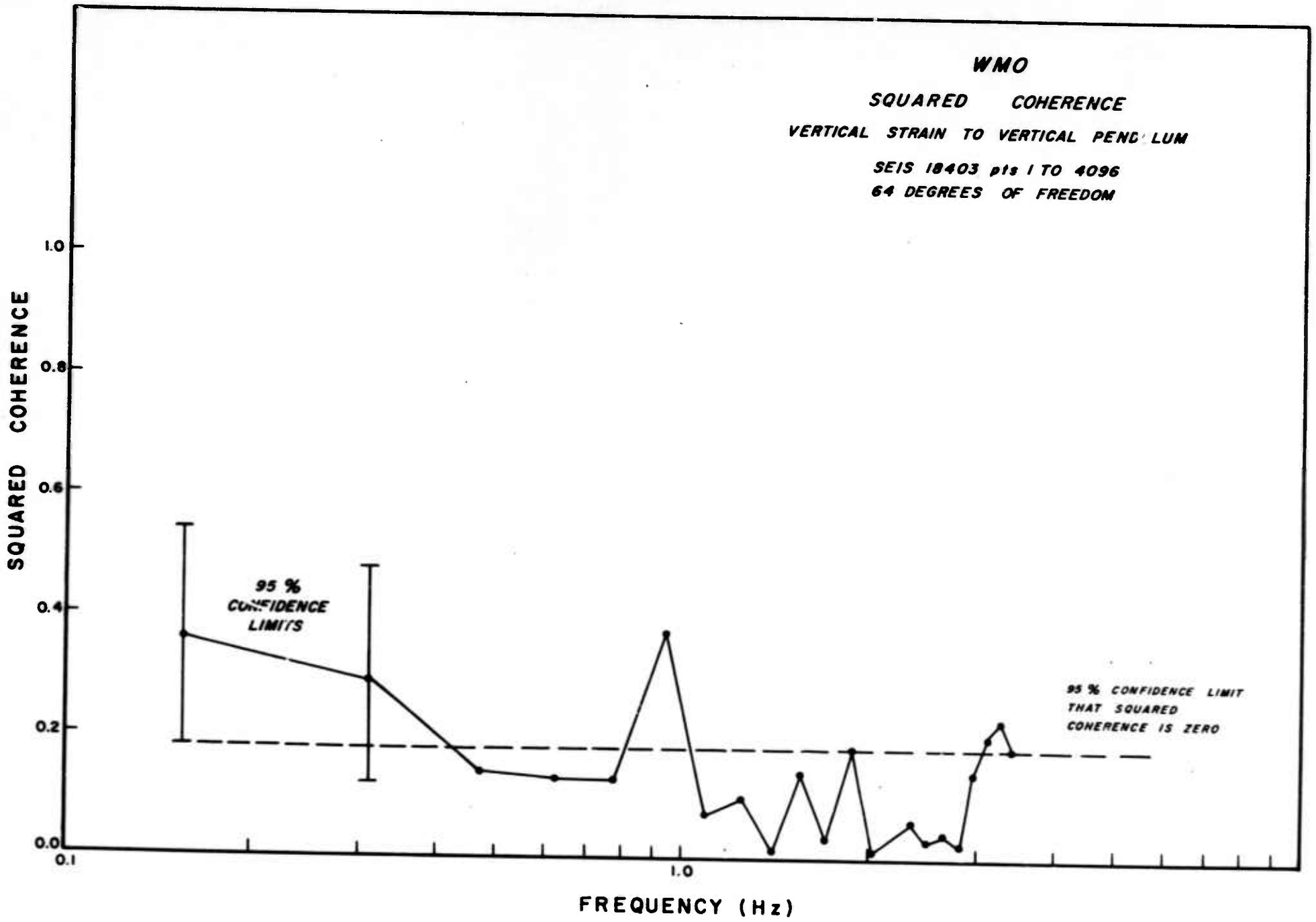

Figure 9. WMO - Squared Coherence - Vertical Strain to Vertical Pendulum.

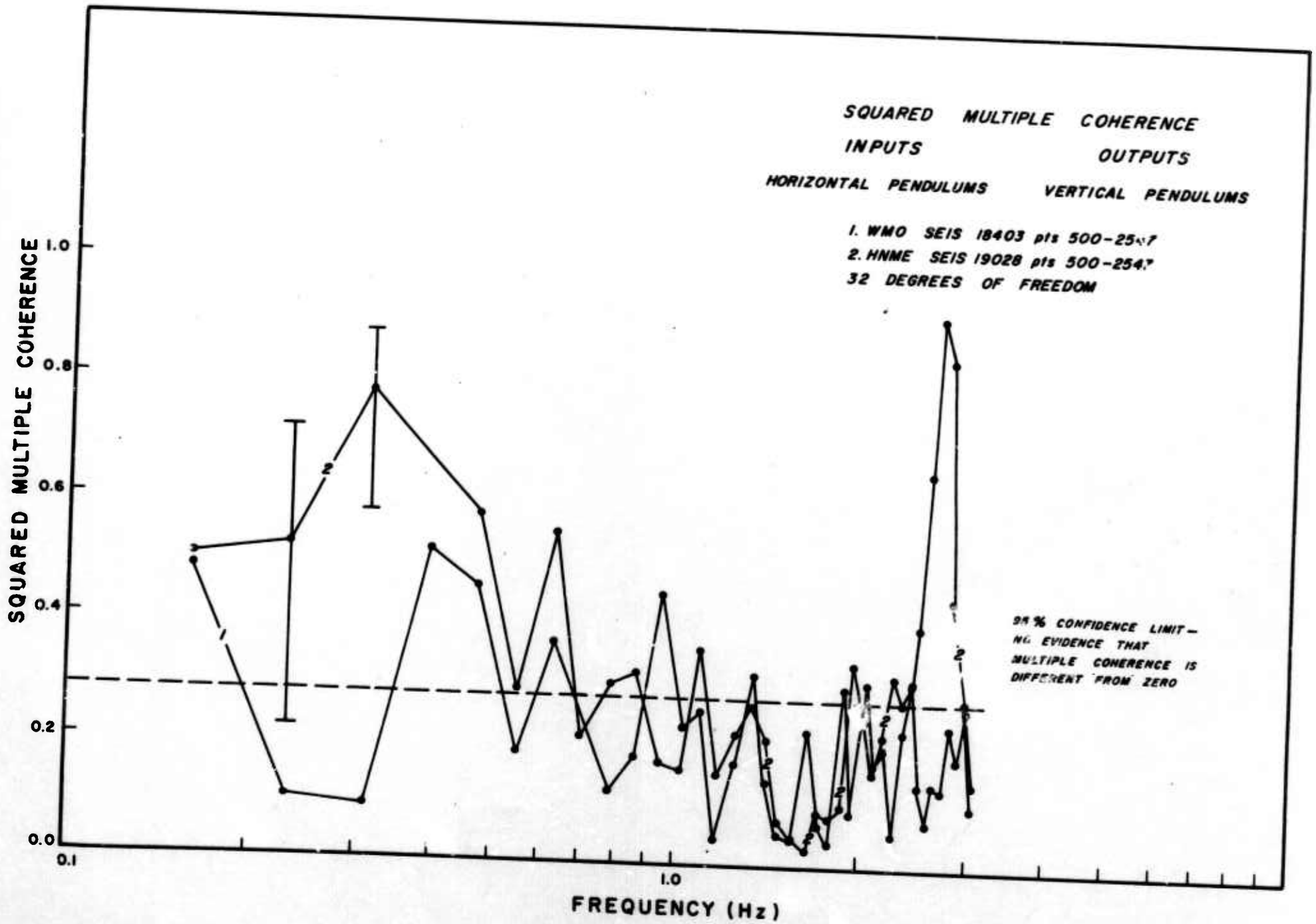

Figure 11. Squared Multiple Coherence - Horizontal Pendulums to Vertical Pendulums.

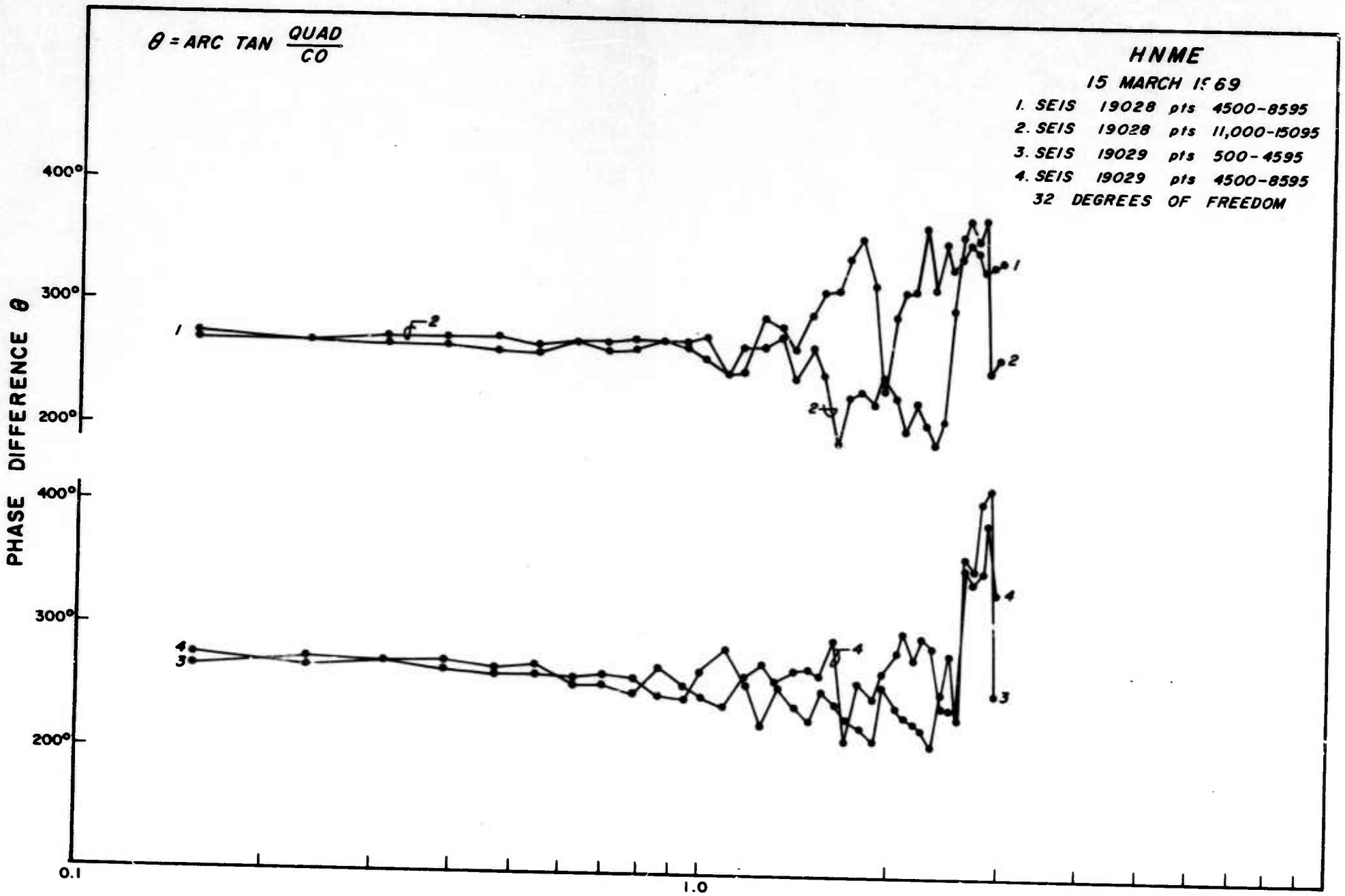

Figure 10. HNME - Phase Difference Vertical Strain-Vertical Pendulum.

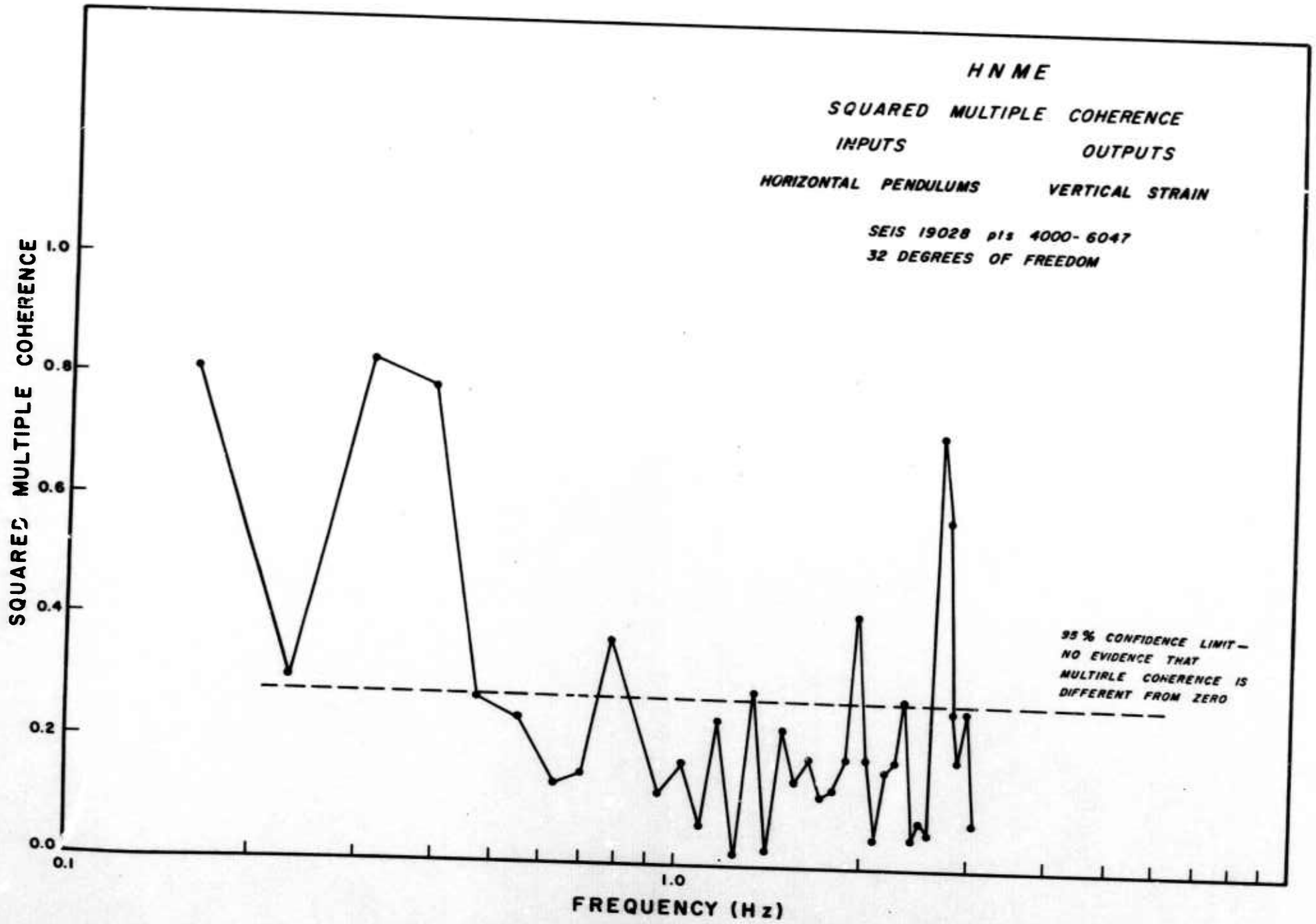

Figure 12. HNME - Squared Multiple Coherence.

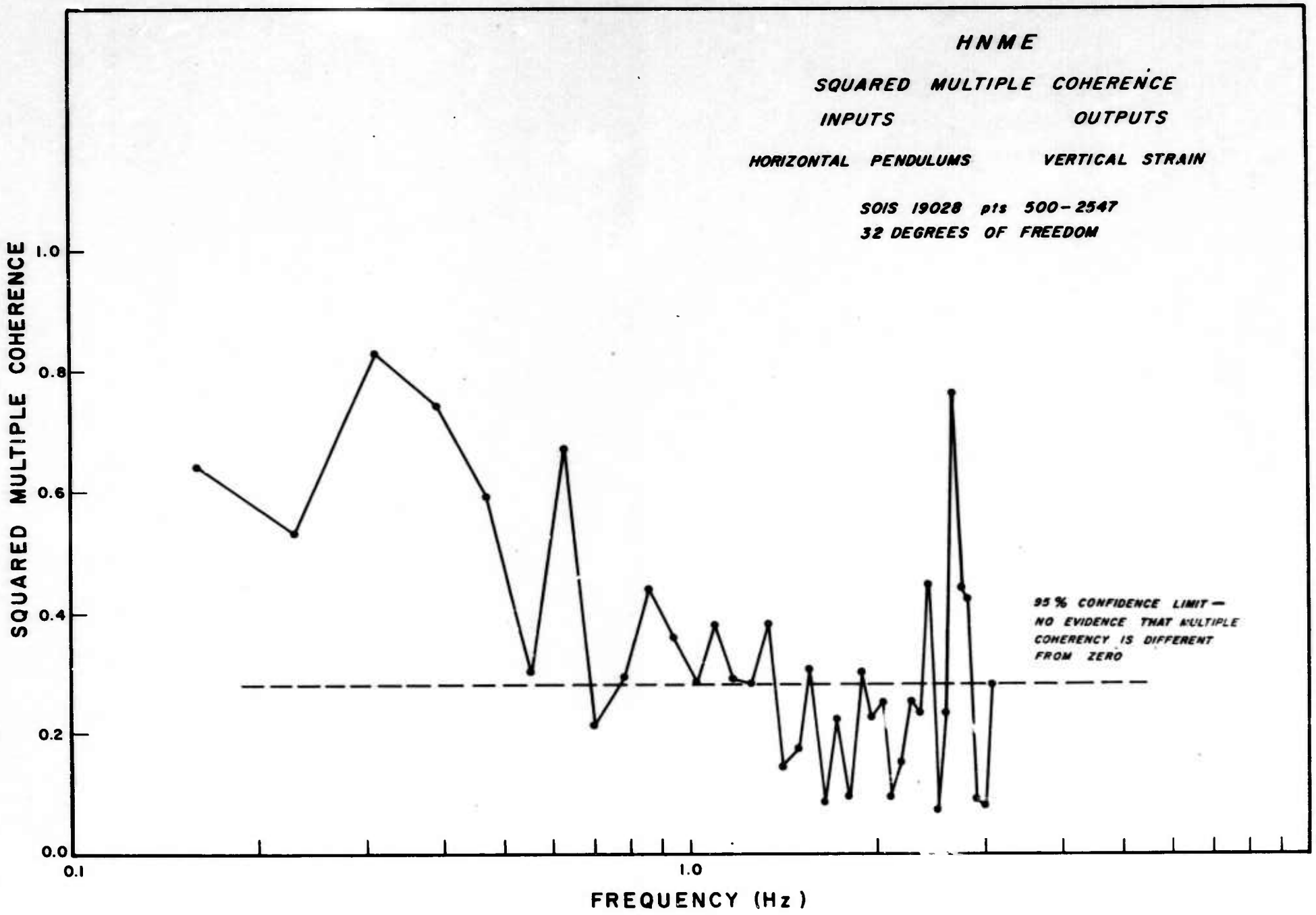

Figure 13. HNME - Squared Multiple Coherence.

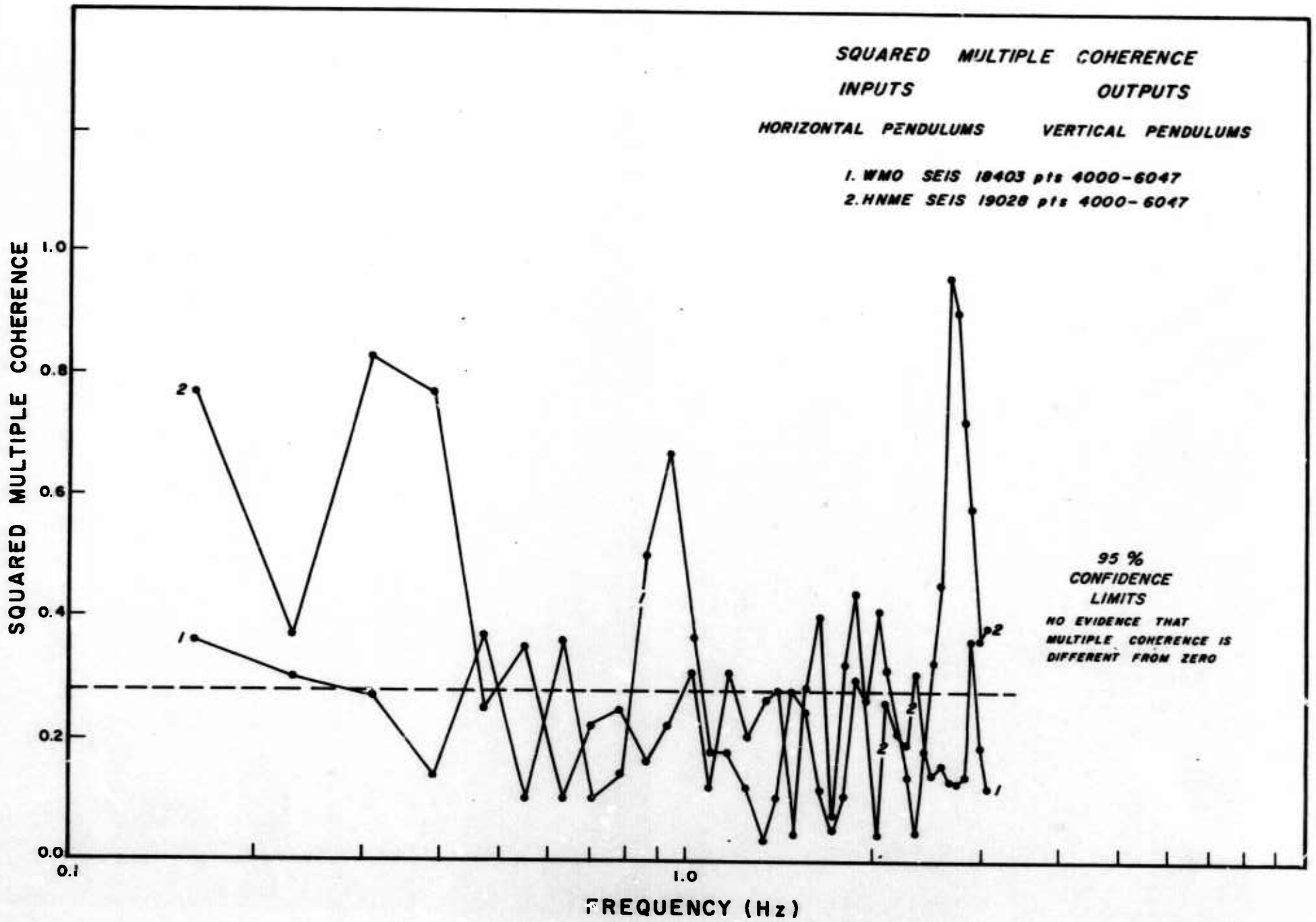

Figure 14. Squared Multiple Coherence - Horizontal Pendulums to Vertical Pendulums.

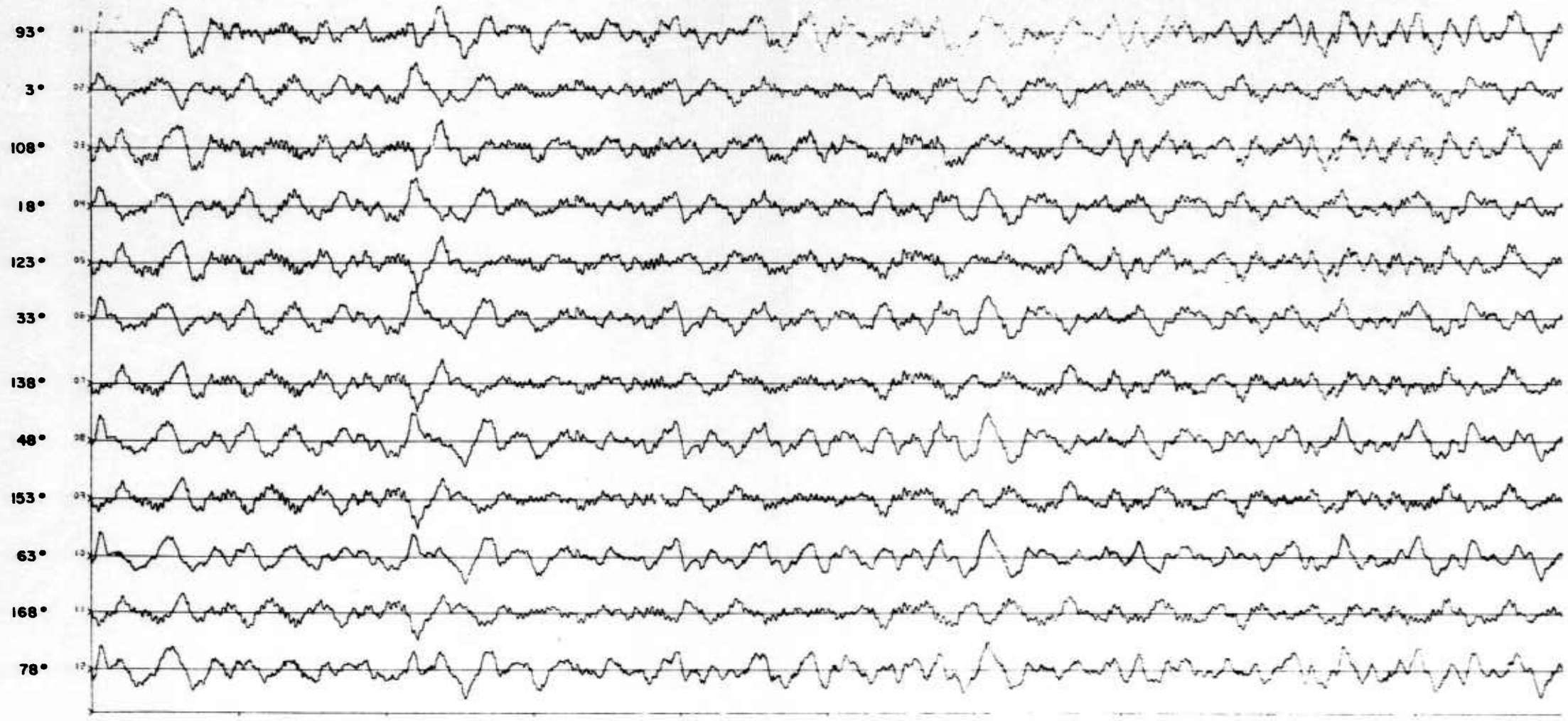

FIGURE 15. HNME - PENDULUM ROTATION.

HNME

PENDULUM ROTATION

SEIS NO 19028, pts 501-2500

ORIGINAL

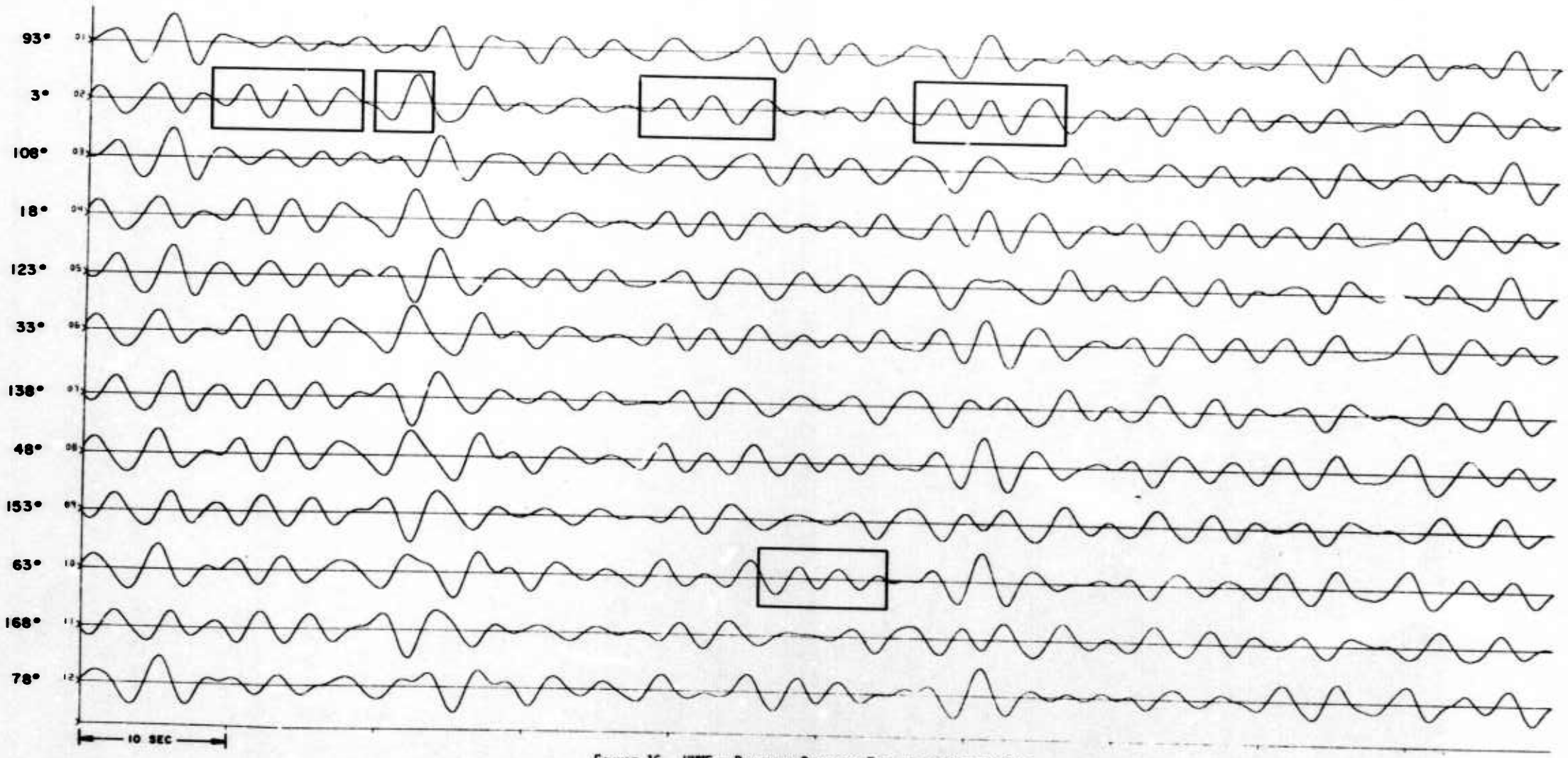

FIGURE 16. HNME - PENDULUM ROTATION FILTERED 0.1 TO 0.5 Hz.

HNME

PENDULUM ROTATION

SEIS NO. 19028, pts 501-2500

FILTERED 0.1 TO 0.5 Hz

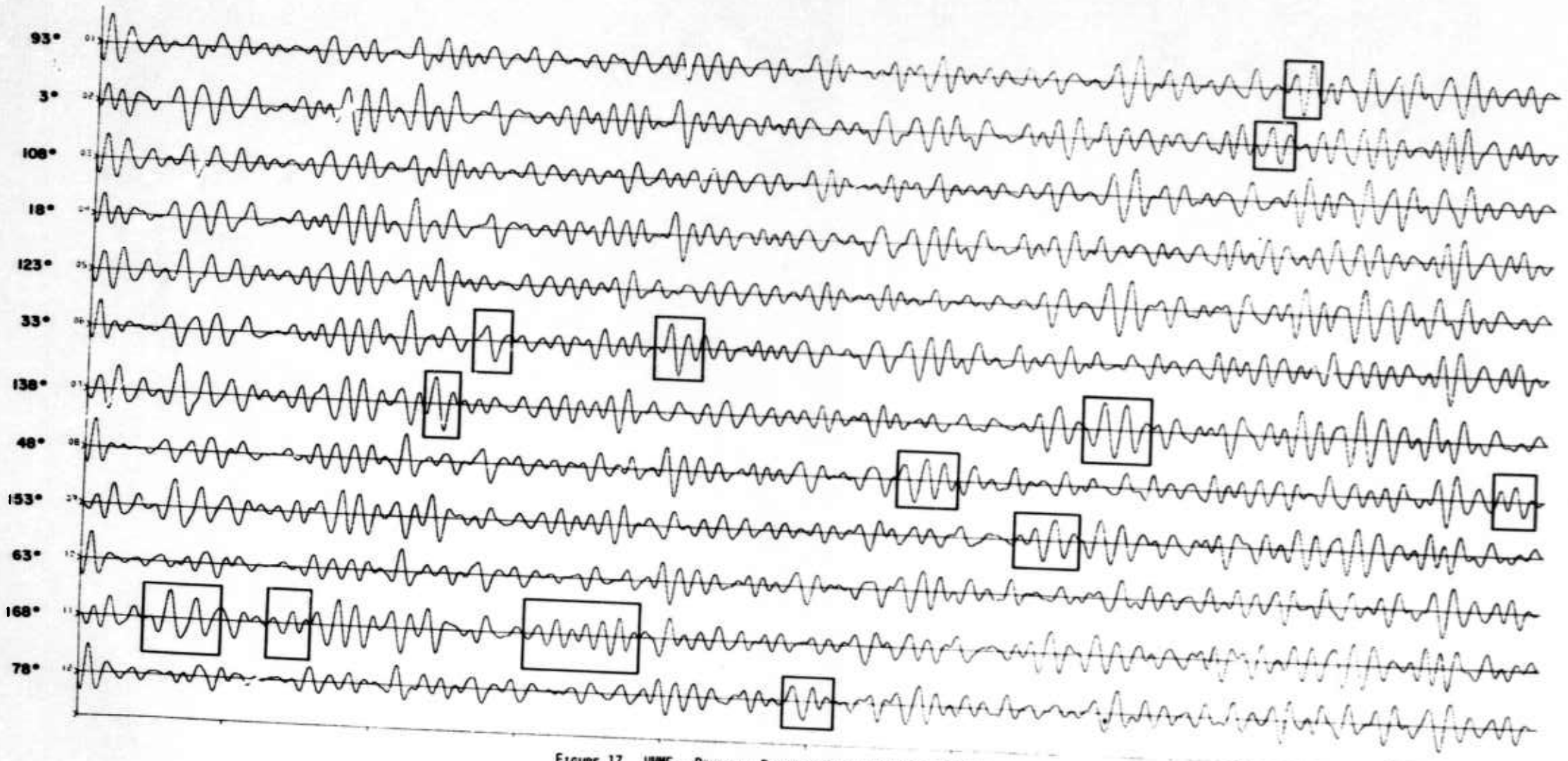

FIGURE 17. HNME - PENDULUM ROTATION FILTERED 0.5 TO 1.2 Hz.

HNME

PENDULUM ROTATION

SEIS NO 19028, pts 501-2500

FILTERED 0.5 TO 1.2 Hz

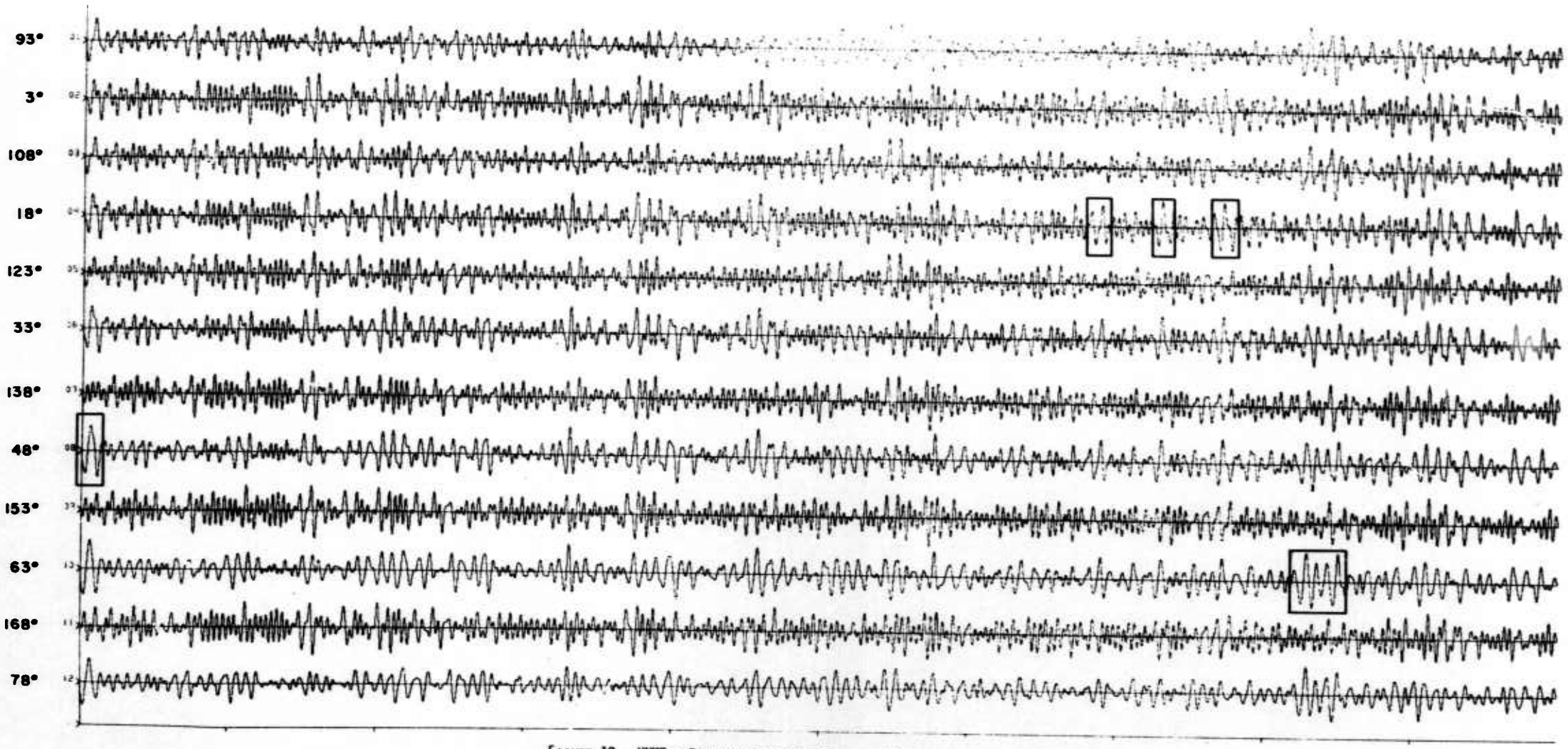

FIGURE 18. IBME - PENDULUM ROTATION FILTERED 1.2 TO 2.4 Hz.

GRAPHIC CONTROLS CORPORATION BUFFALO, NEW YORK

HNME

PENDULUM ROTATION

SEIS NO. 19028, pts 501-2500

FILTERED 1.2 TO 2.4Hz

RECORDING CHARTS GRAPHIC CONTROLS CORPORATION BUFFALO, NEW YORK

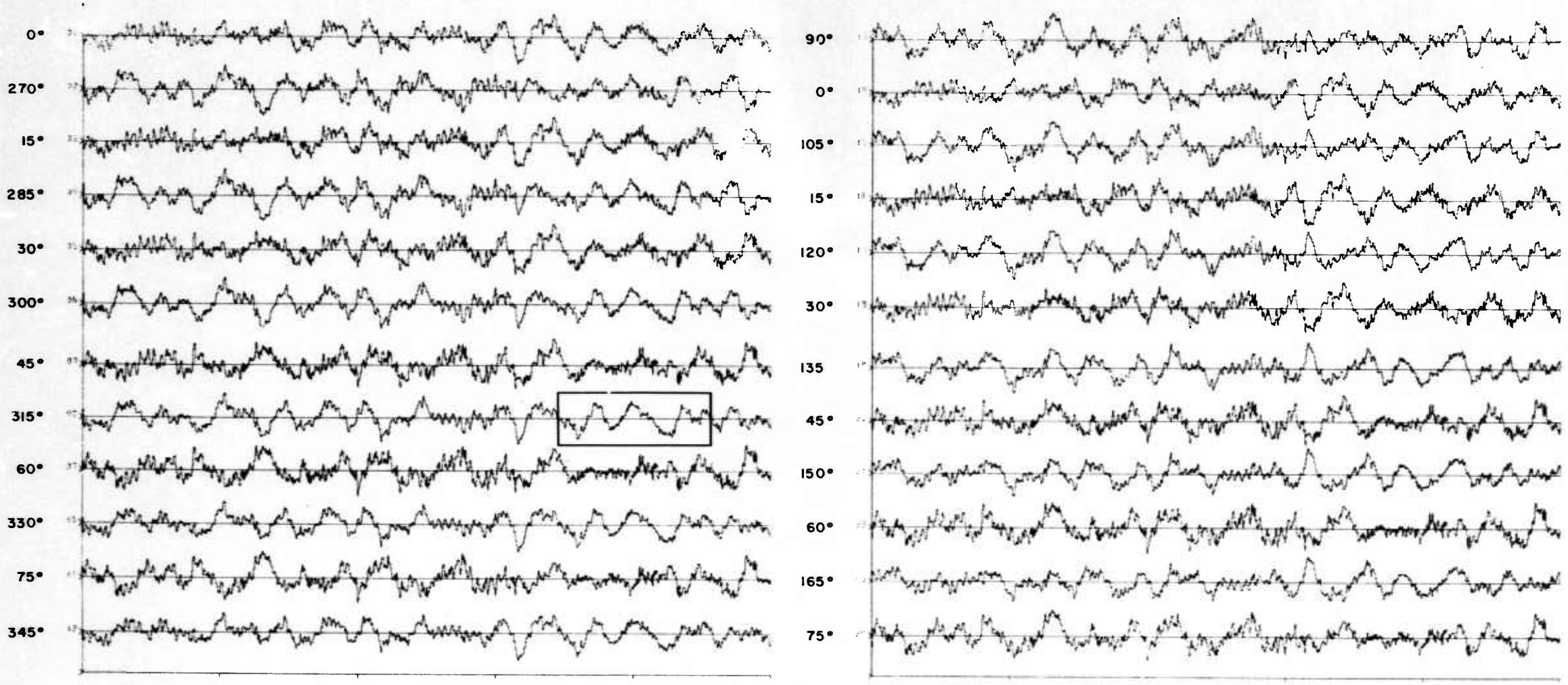

FIGURE 19. WMO - PENDULUM ROTATION.

RECORDING CHARTS GRAPHIC CONTROLS CORPORATION

WMO
PENDULUM ROTATION
SEIS 18403 pts 50 TO 1050
ORIGINAL

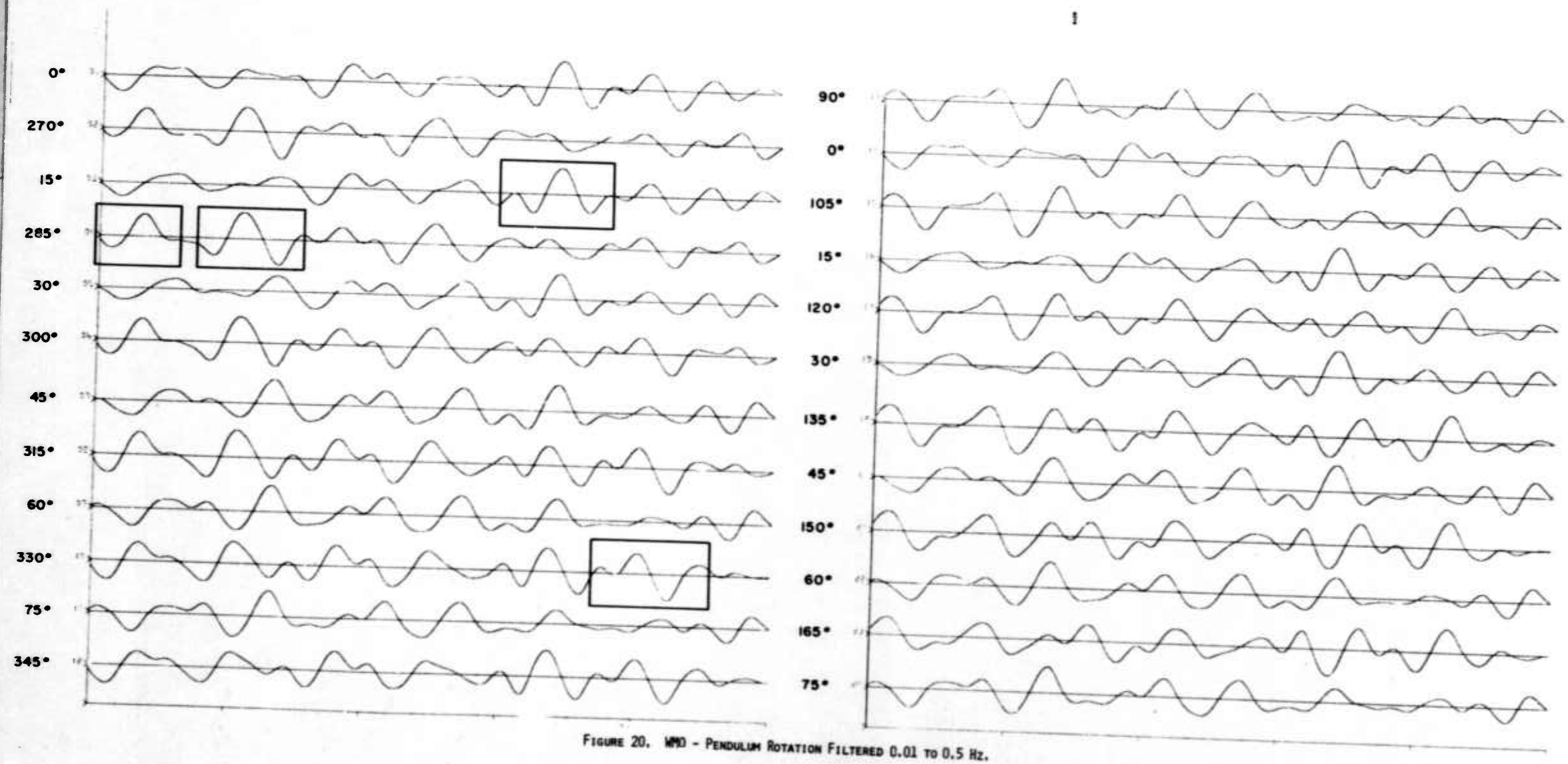

FIGURE 20. WMO - PENDULUM ROTATION FILTERED 0.01 TO 0.5 Hz.

WMO

PENDULUM ROTATION

SEIS 18403 pts 50 TO 1050

0.01 TO 0.5 Hz

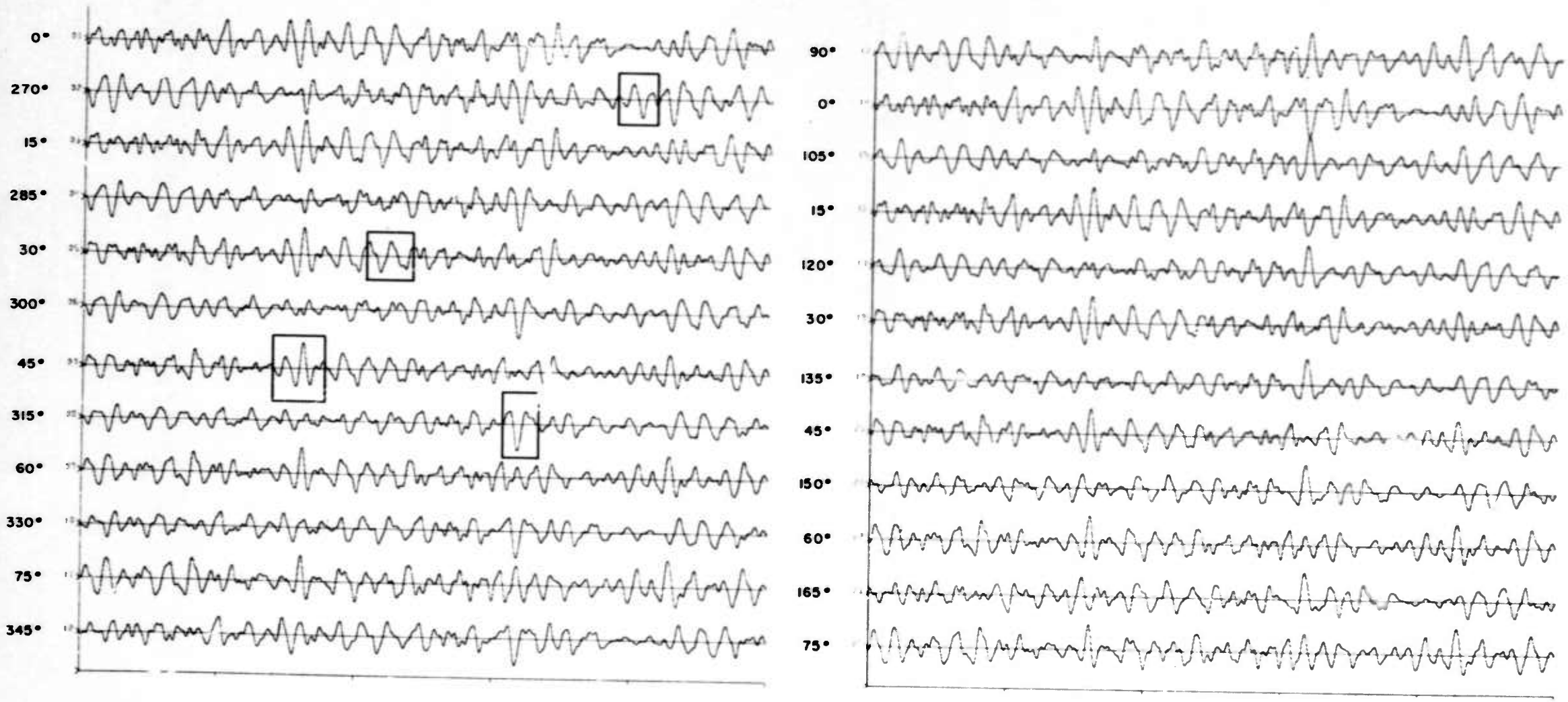

FIGURE 21. WMO - PENDULUM ROTATION FILTERED 0.5 TO 1.6 Hz.

WMO

PENDULUM ROTATION

SEIS 18403 pts 50 TO 1050

0.5 TO 1.6 Hz

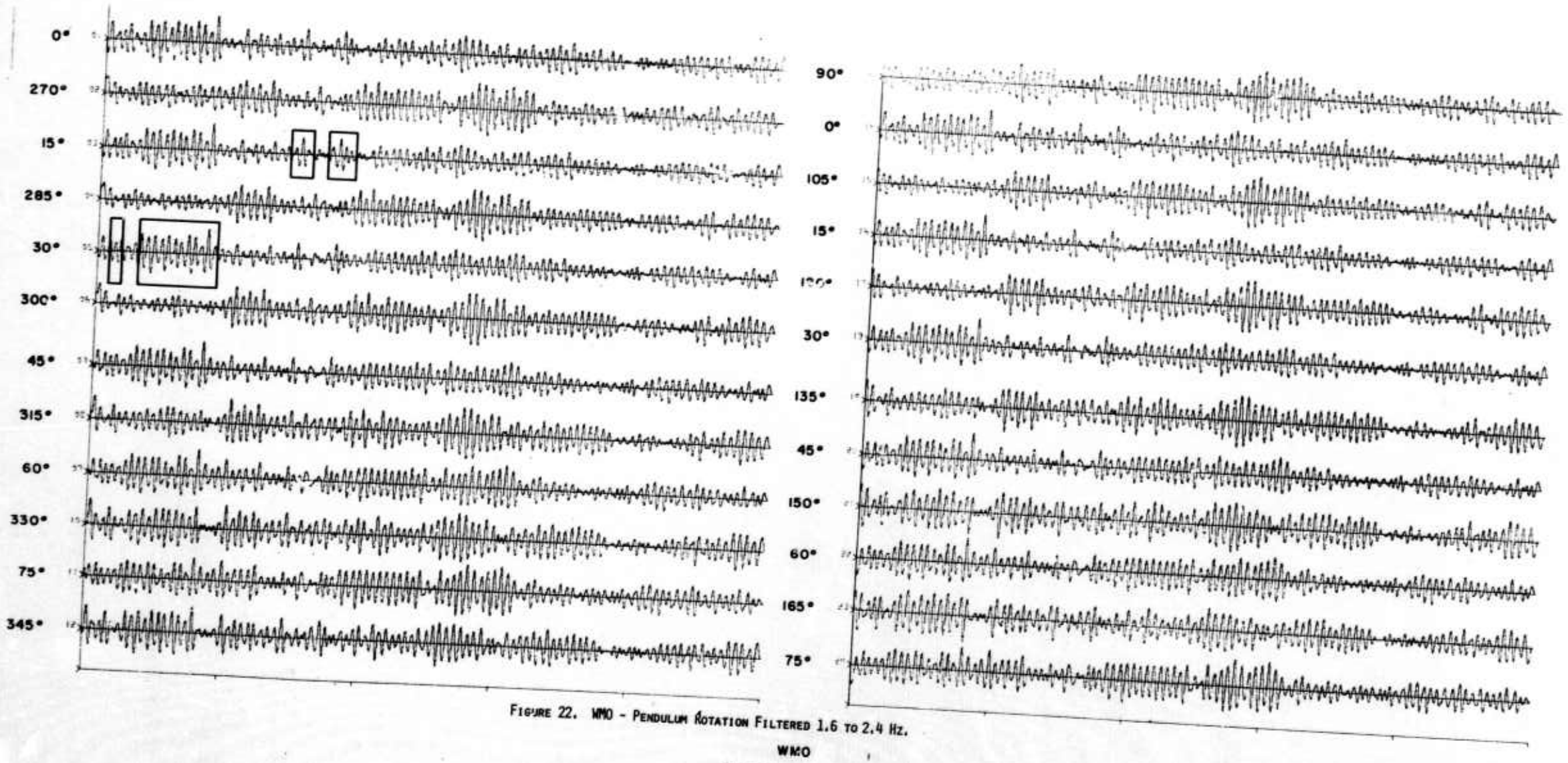

FIGURE 22. WMO - PENDULUM ROTATION FILTERED 1.6 TO 2.4 Hz.

WMO

PENDULUM ROTATION

SEIS 18403 pts 50 TO 1050

1.6 TO 2.4 Hz

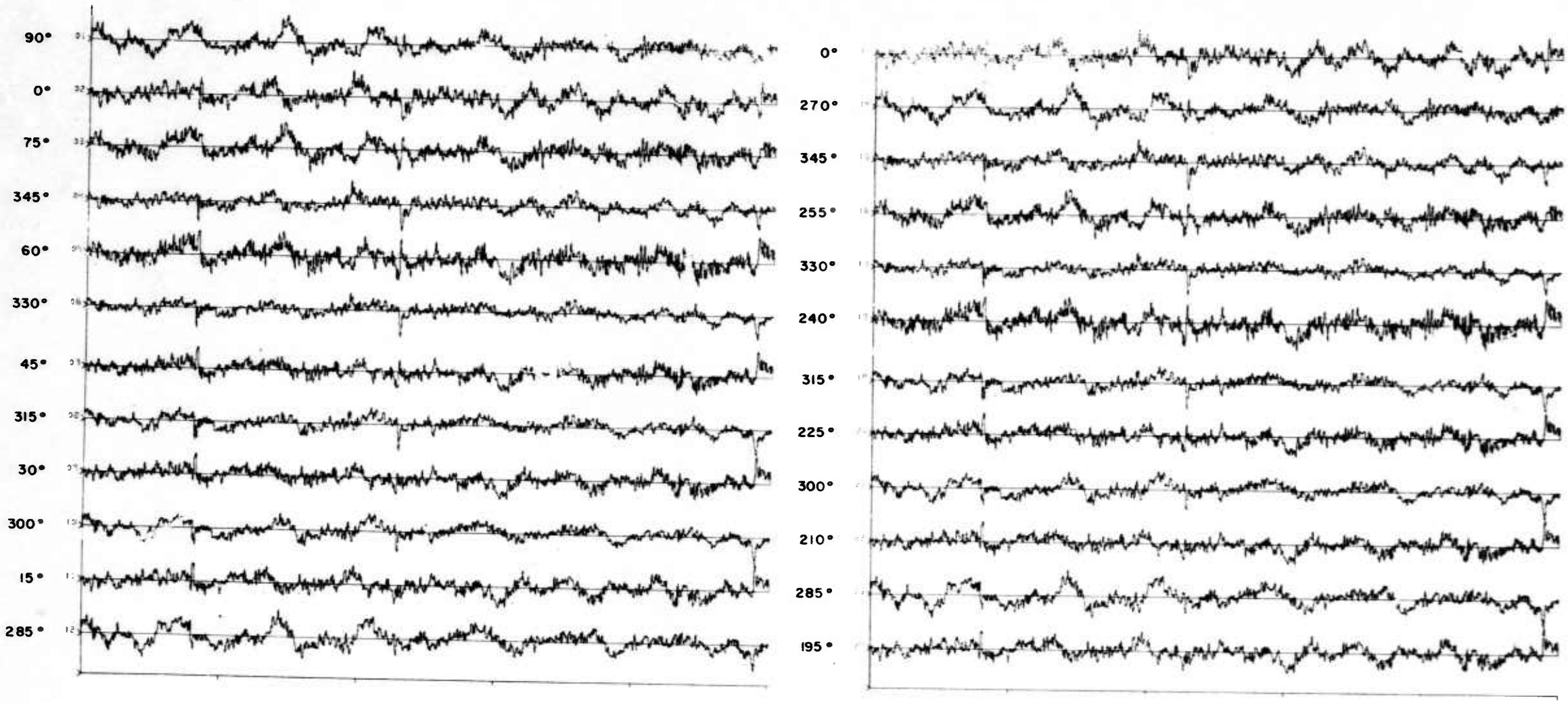

FIGURE 23. WMO - STRAIN ROTATION.

WMO

STRAIN ROTATION

SEIS NO. 18403 pts 50-105

ORIGINAL

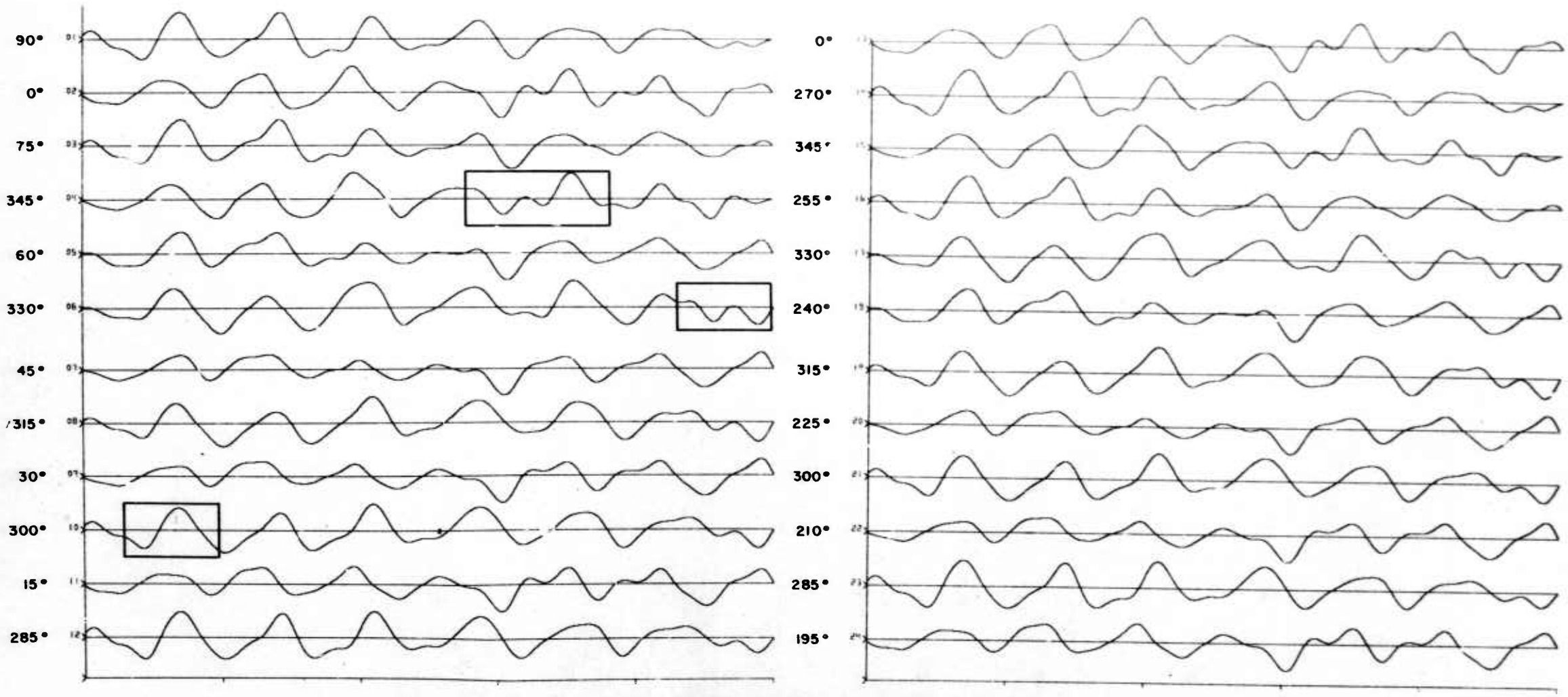

FIGURE 24. WMO - STRAIN ROTATION FILTERED 0.01 TO 0.5 Hz.

WMO

STRAIN ROTATION

SEIS NO. 18403 pts 50-1050

FILTERED 0.01 TO 0.5 Hz

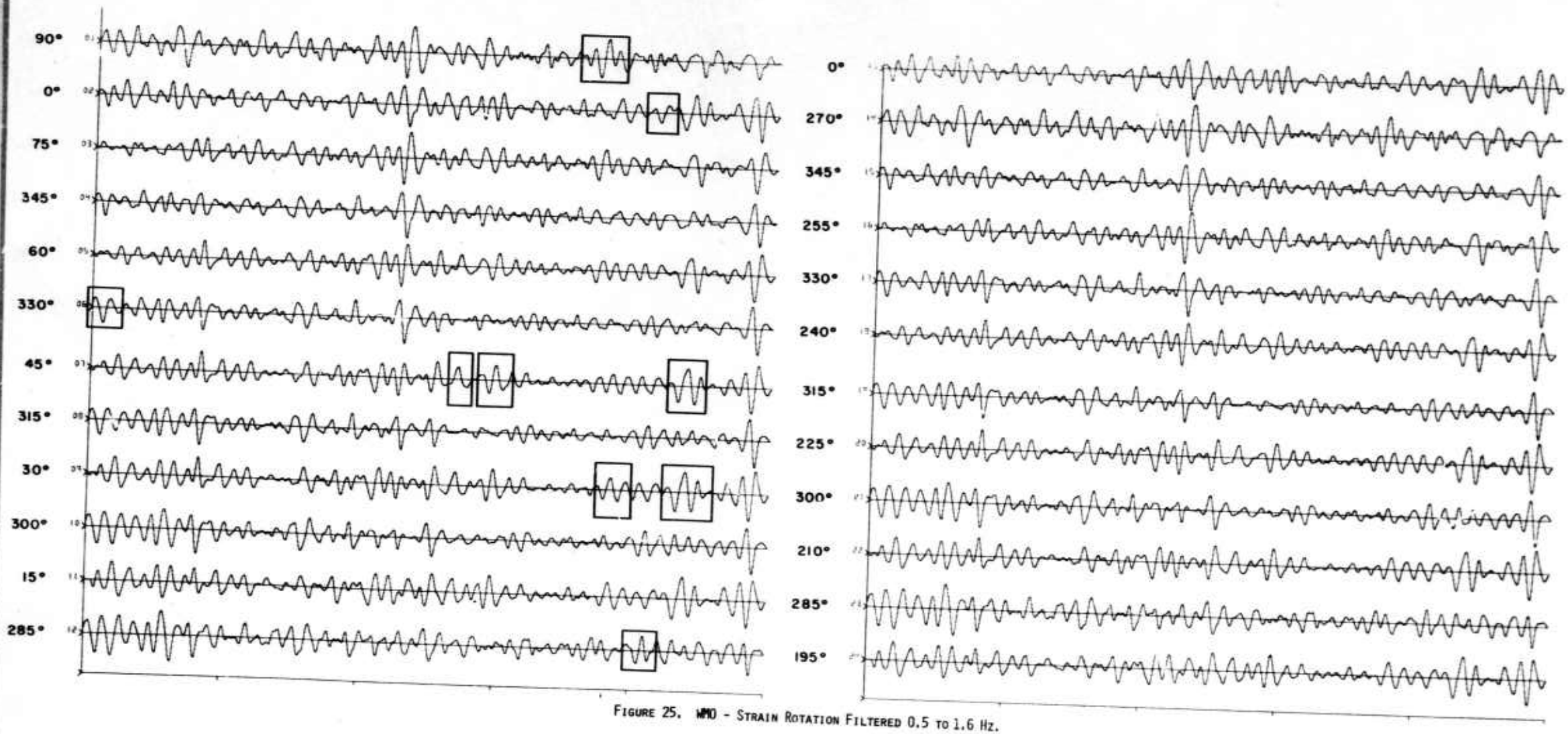

FIGURE 25. WMO - STRAIN ROTATION FILTERED 0.5 TO 1.6 Hz.

WMO

STRAIN ROTATION

SEIS NO. 18403 pts 50-1050

FILTERED 0.5 TO 1.6 Hz

RECORDING CHARTS GRAPHIC CONTROLS CORPORATION BUFFALO, N. Y. U.S.A.

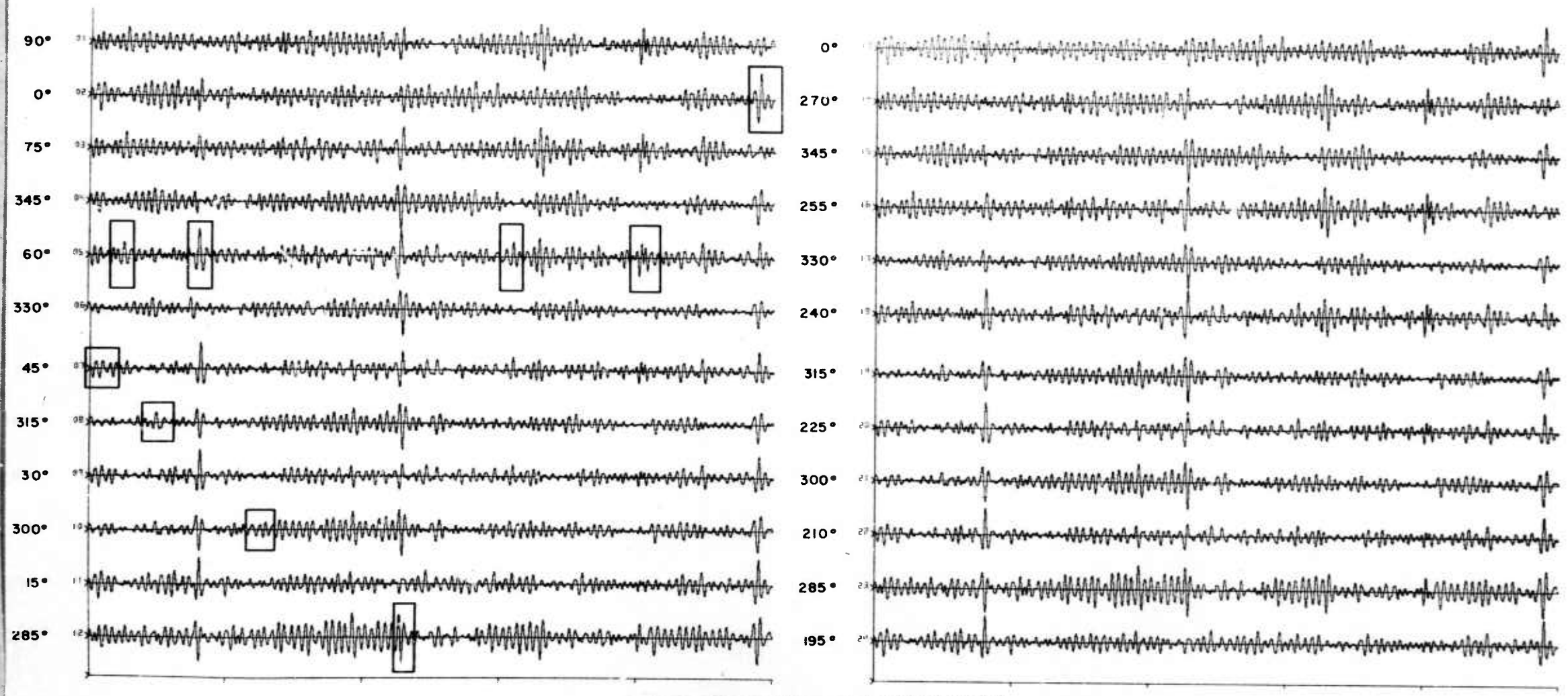

FIGURE 26. WMO - STRAIN ROTATION FILTERED 1.6 TO 2.4 Hz.

WMO

STRAIN ROTATION

SEIS NO. 18403 pts 50-1050

FILTERED 1.6 TO 2.4 Hz

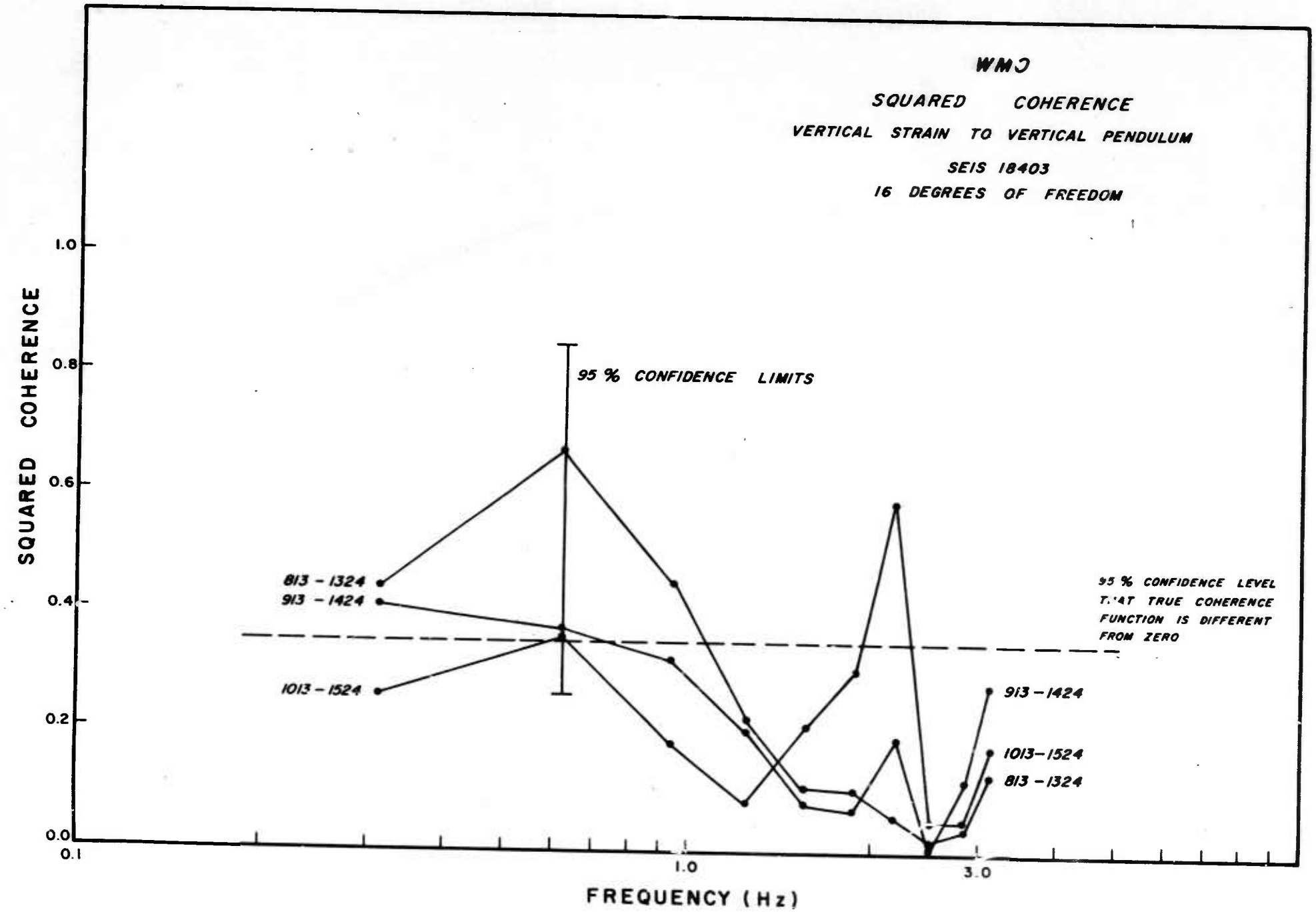

Figure 27. KNO - Squared Coherence - Vertical Strain to Vertical Pendulum.

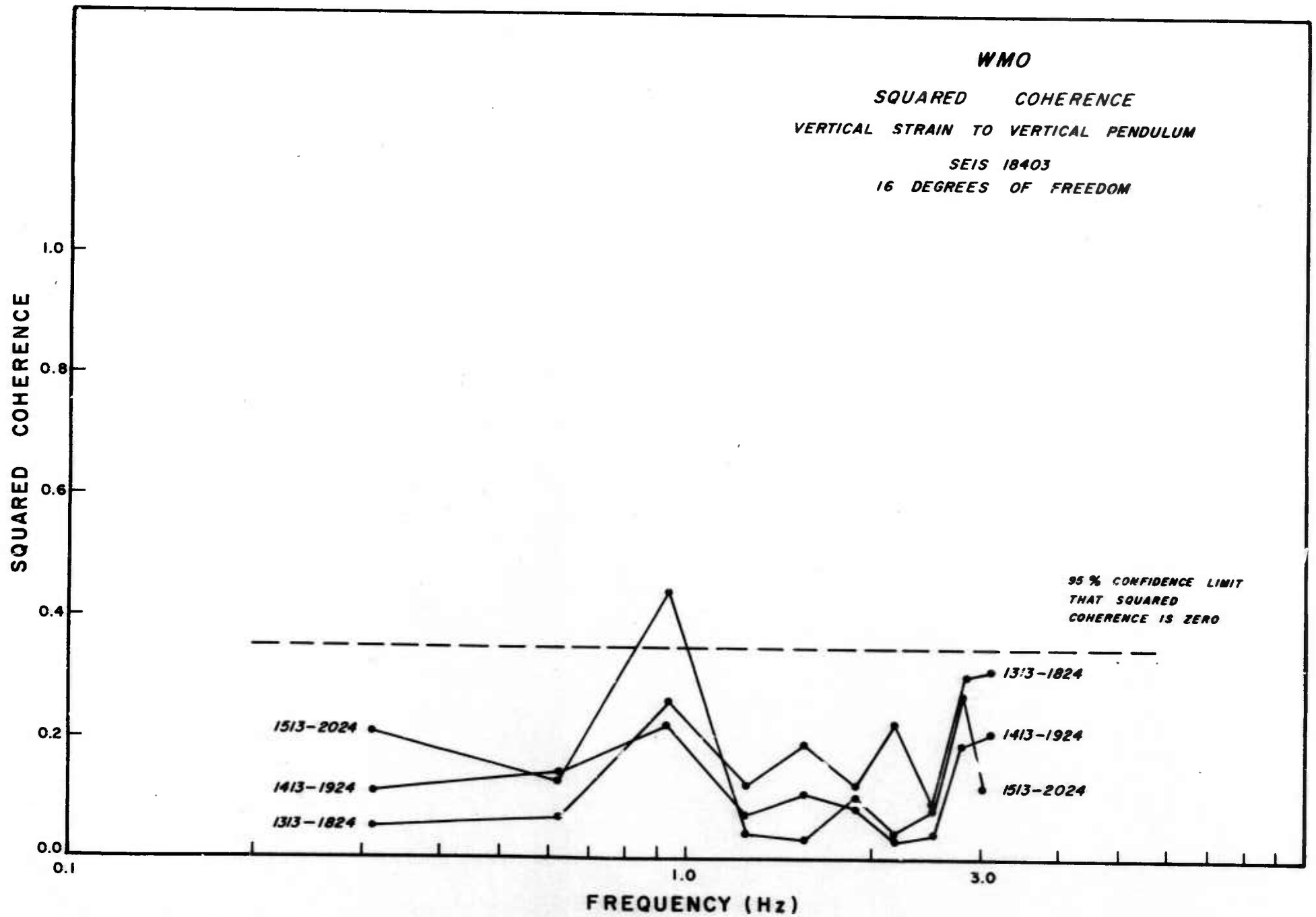

Figure 28. WMO - Squared Coherence - Vertical Strain to Vertical Pendulum.

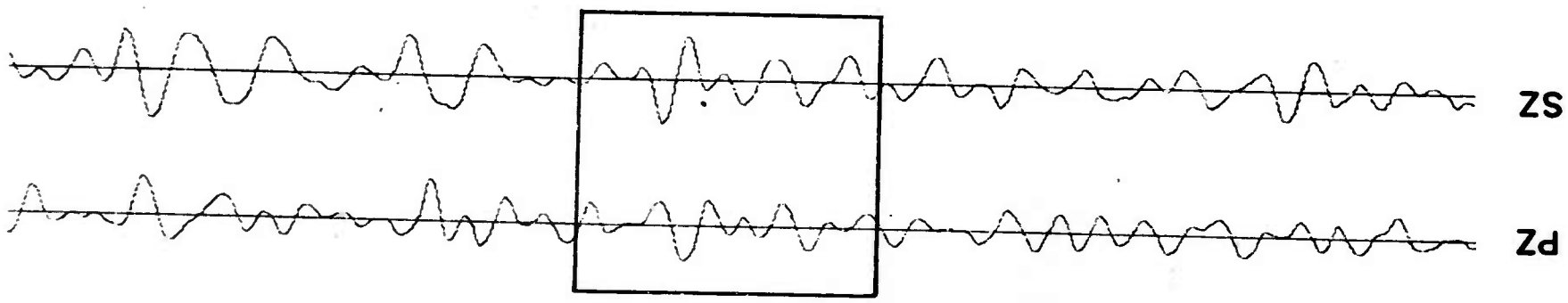

Figure 29. WMO - Detail of Coherent Noise.

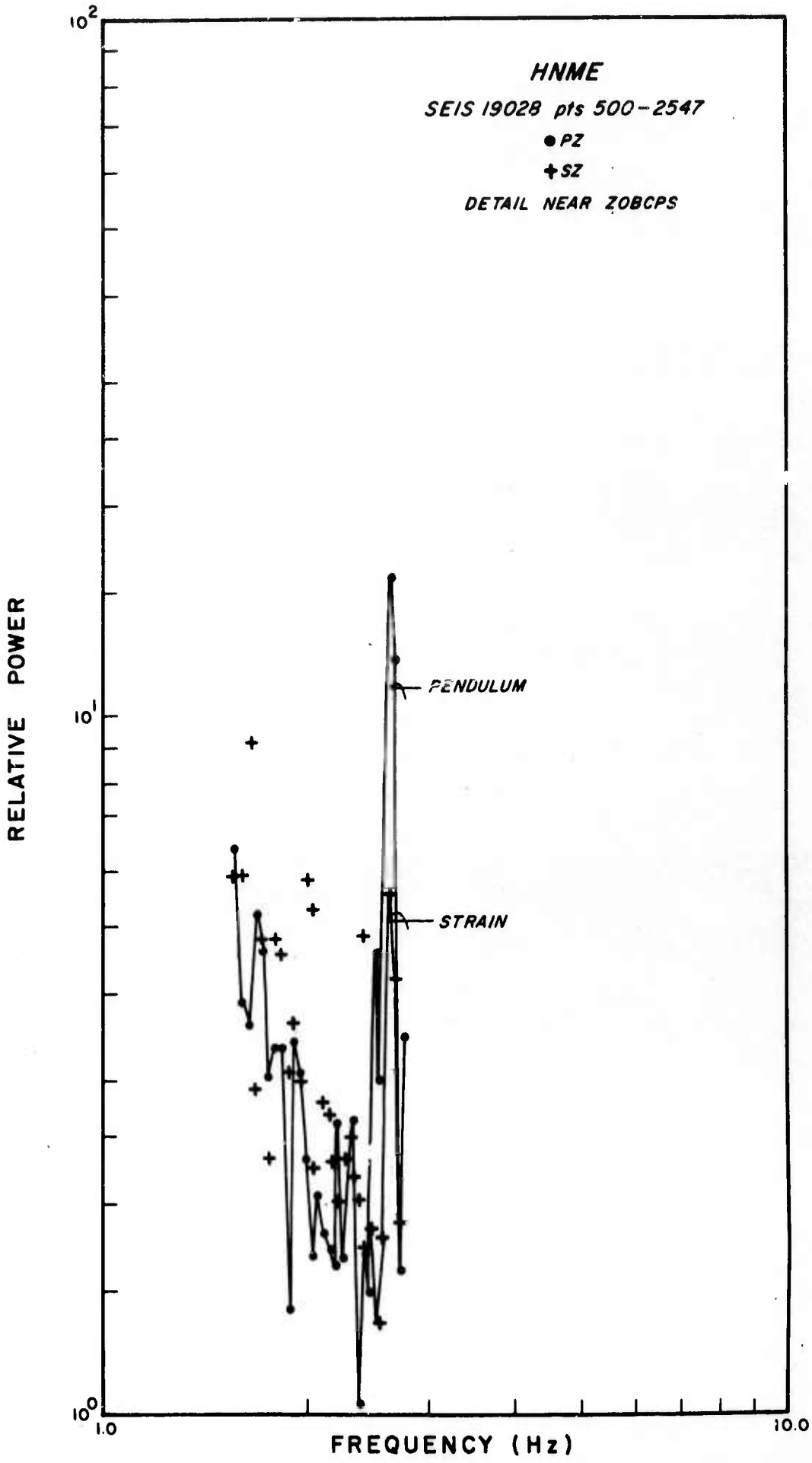

Figure 30. HNME - Relative Power Spectra-Vertical Strain and Vertical Pendulum.

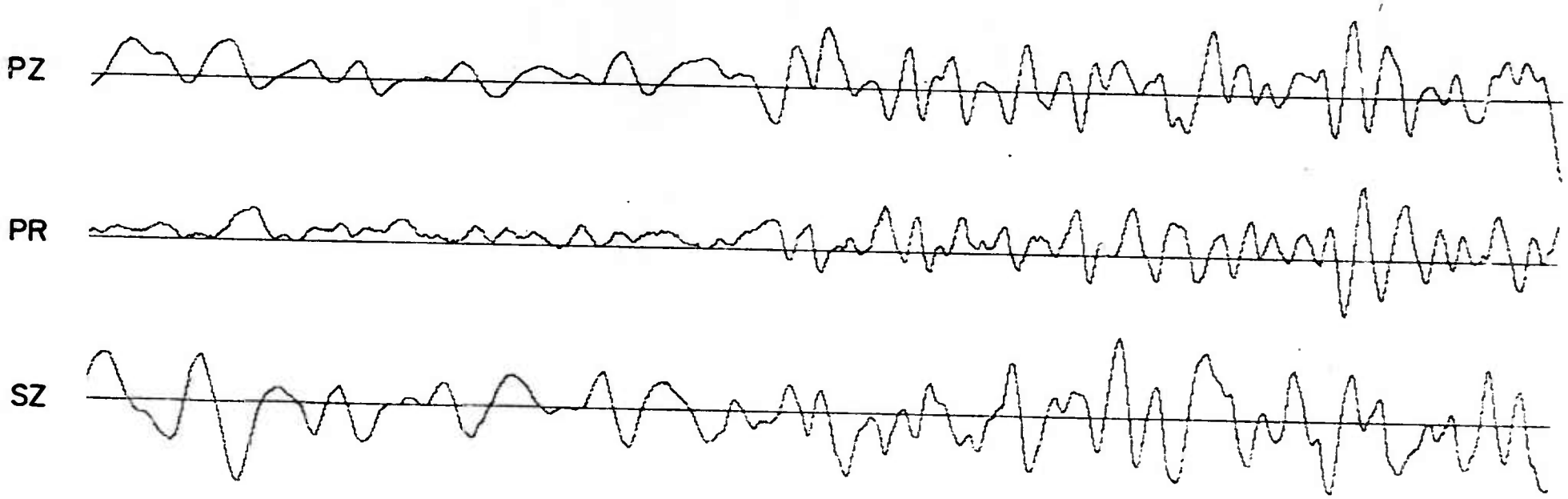

Figure 31. P-Wave Phase Comparison.

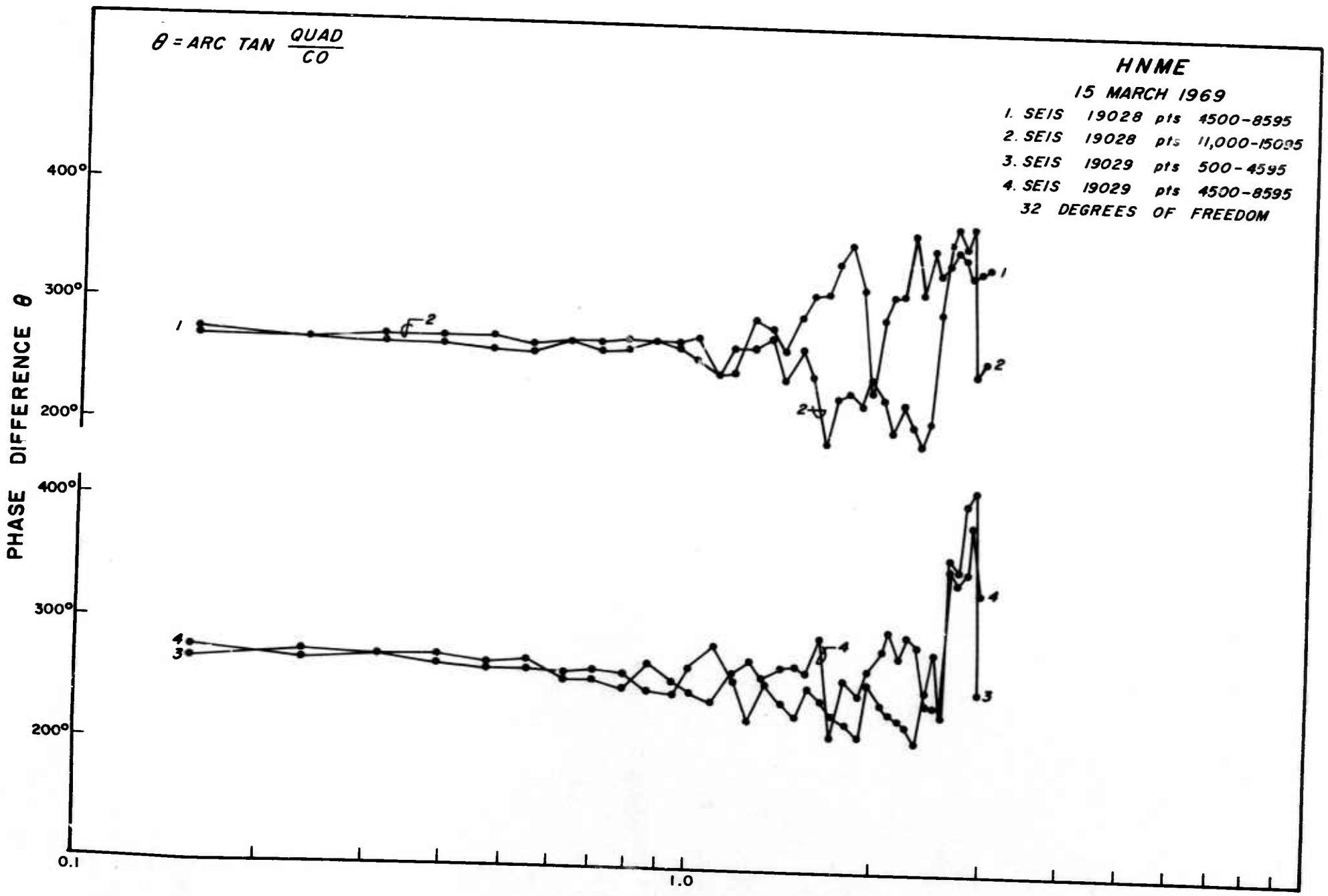

Figure 32. HNME - Phase Difference Vertical Strain-Vertical Pendulum.

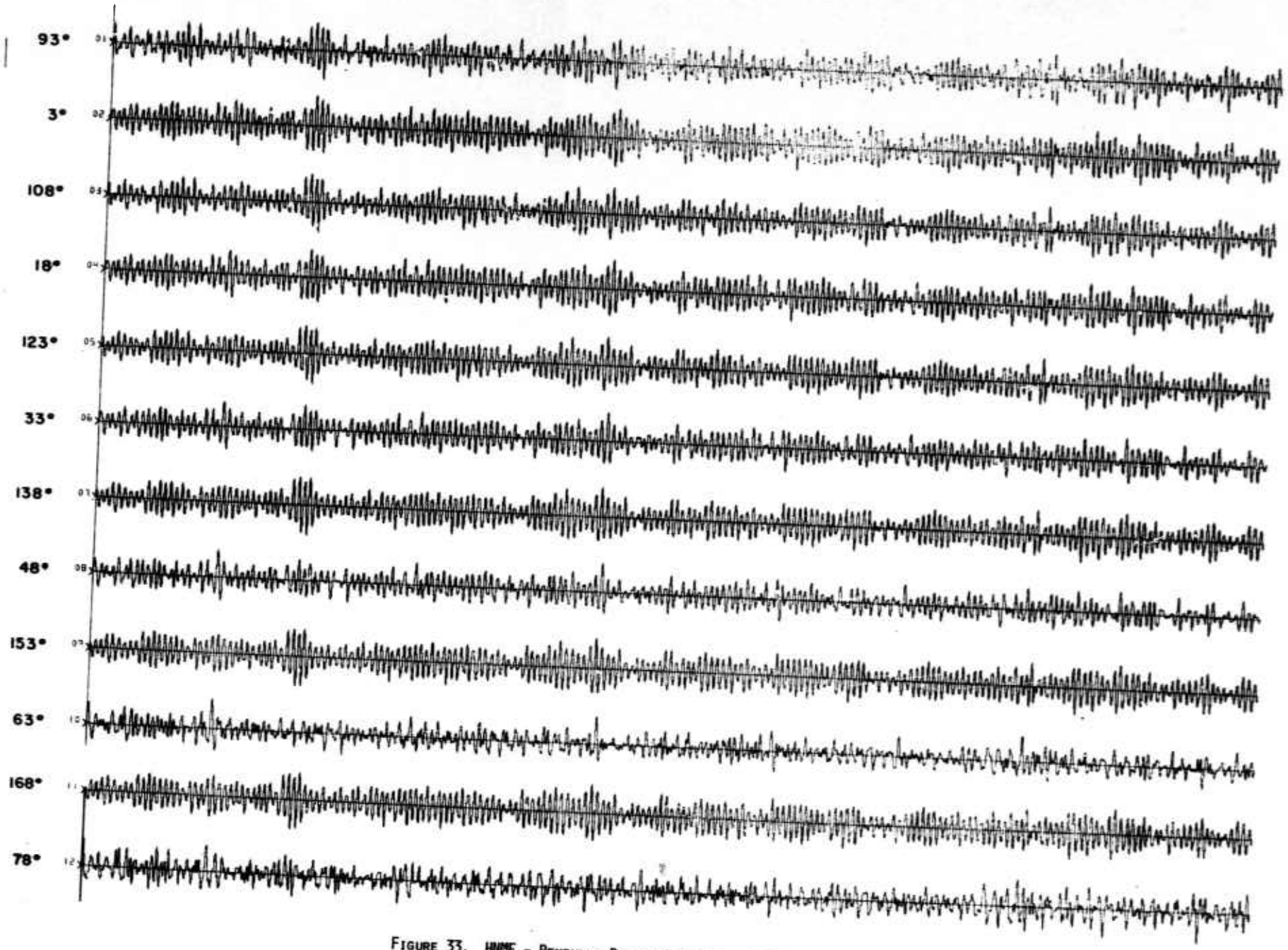

FIGURE 33. HNME - PENDULUM ROTATION FILTERED 1.3 Hz TO 5.2 Hz.

HNME

PENDULUM ROTATION

SEIS NO. 19028, pts 501-2500

FILTERED 1.3 TO 5.2 Hz

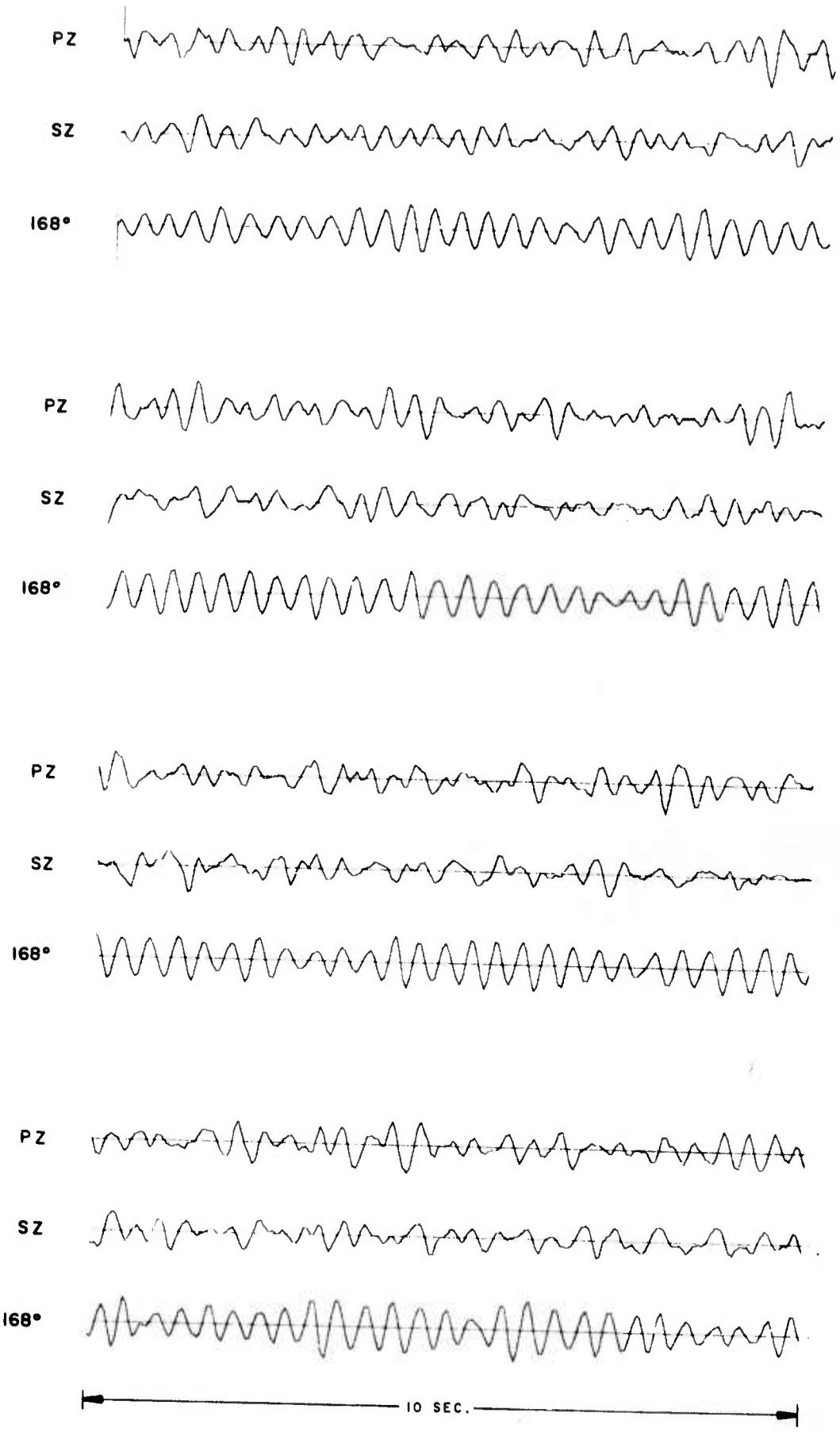

Figure 34. HNME - Phase Comparison - 2.6 Hz.

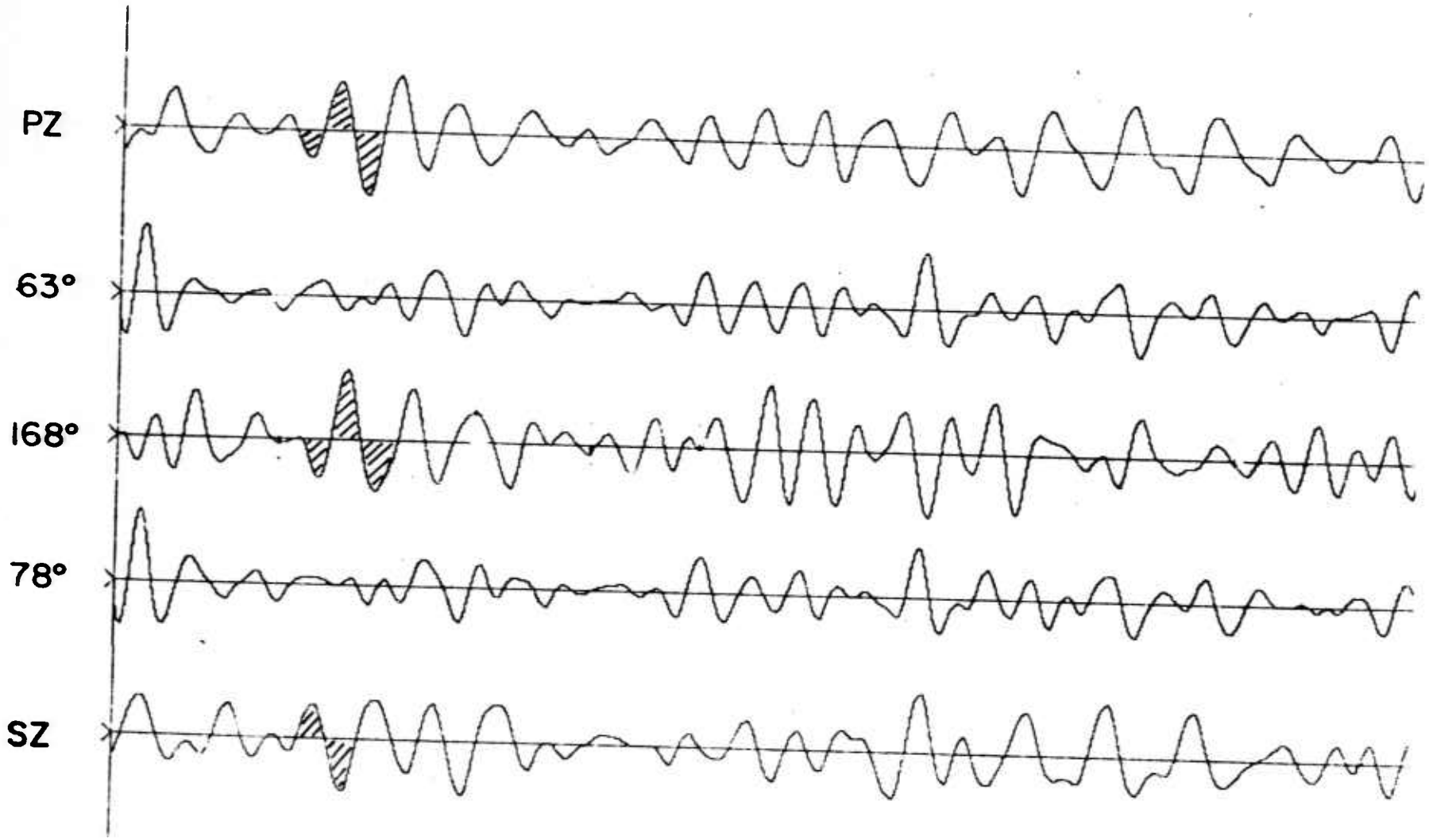

Figure 35. HNME - Phase Comparison (0.5-1.2 Hz).

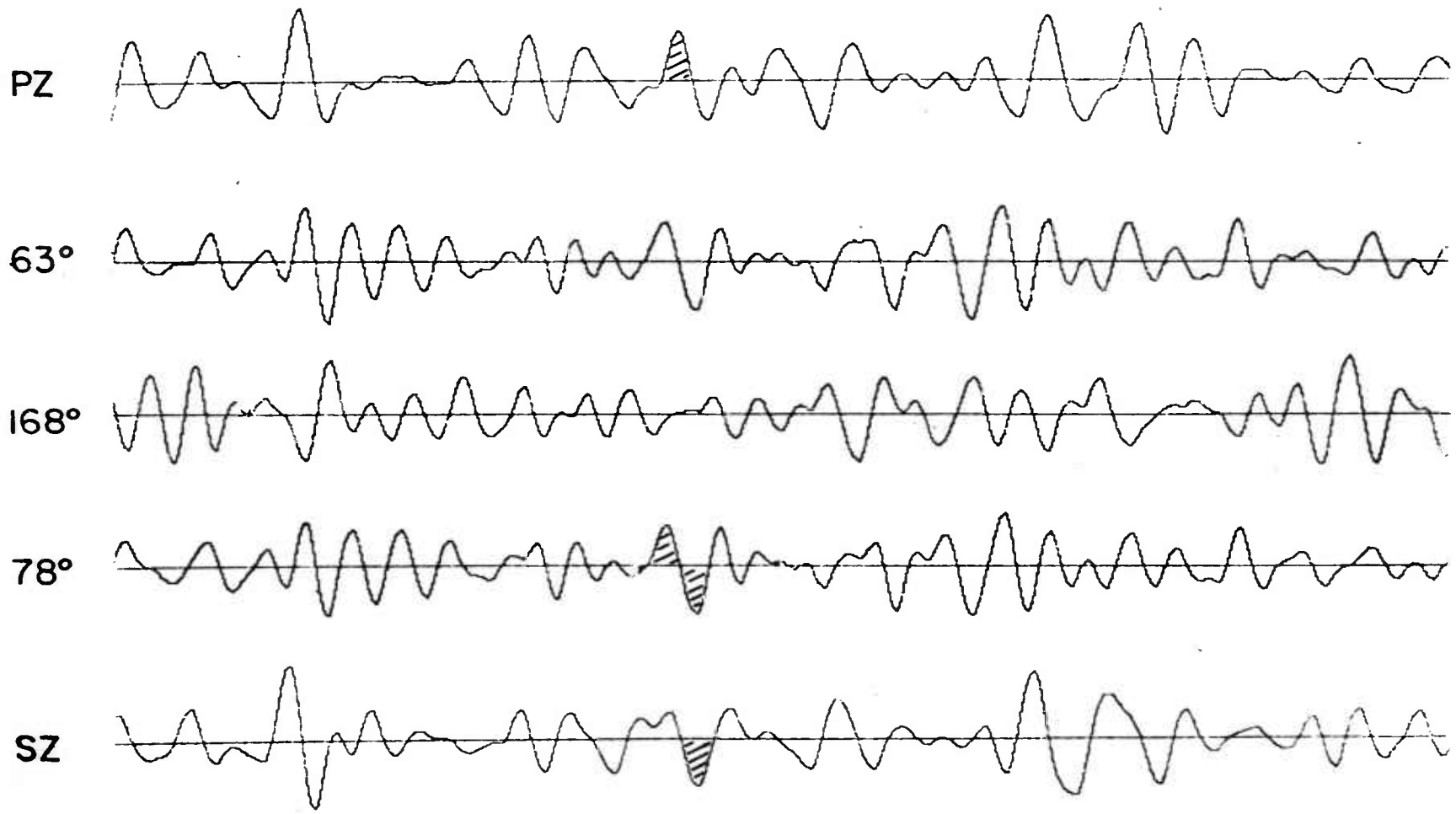

Figure 36. HNME - Phase Comparison (0.5-1.2 Hz).

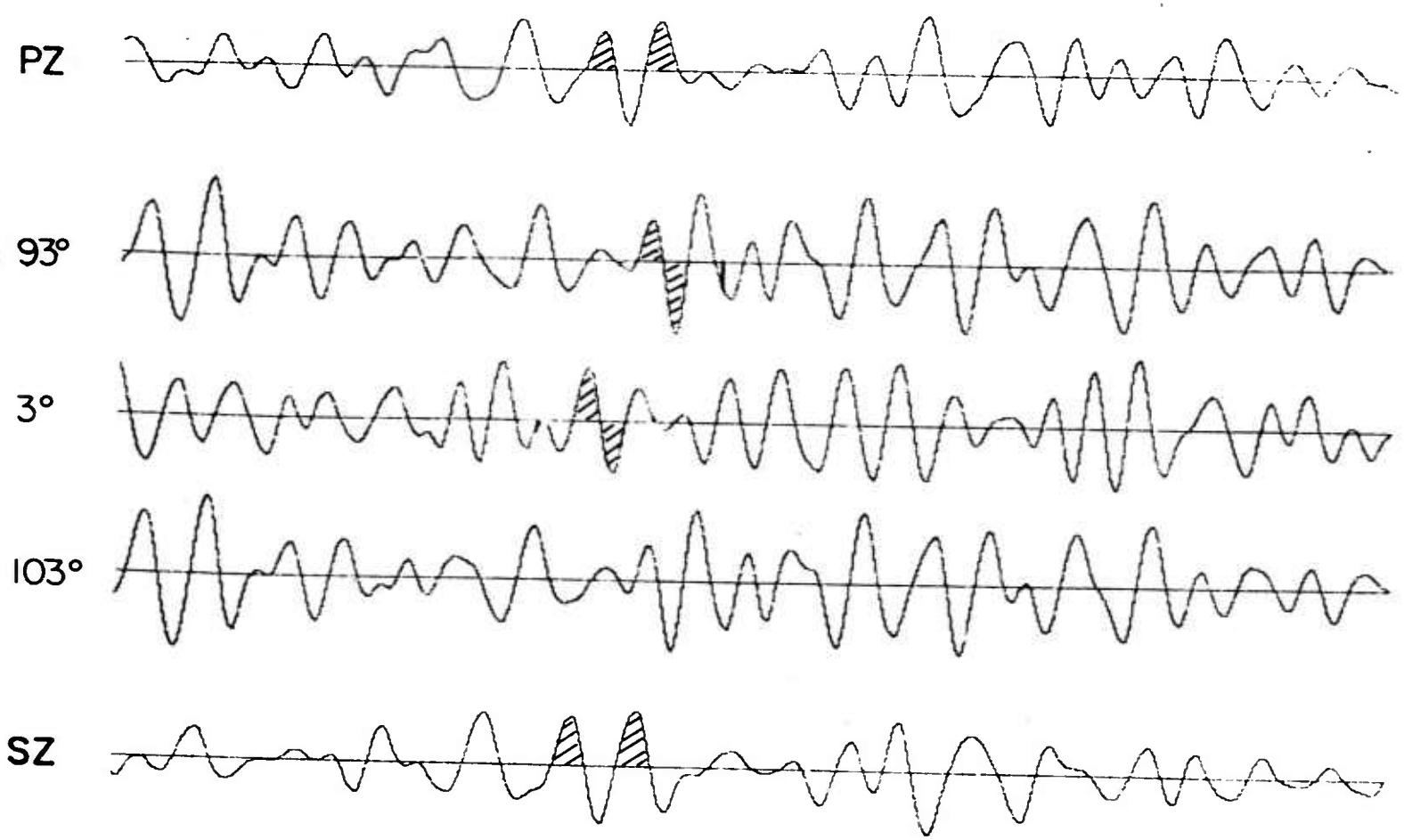

Figure 37. HNME - Phase Comparison (0.5-1.2 Hz).

APPENDIX I

Data Used in Preparation of Report

Seis. 18403 WMO 16,000 points beginning at 0638 27 January 1969 - includes earthquake in Soviet Arctic East of Severnaya Zemlya.

Seis. 18736 HNME 16,000 points beginning at 0520 28 February 1969 noise.

Seis. 18767 FOX 16,000 points beginning 0452 22 November 1968 noise.

Seis. 18774 HNME 16,000 points beginning 0425 28 February 1969 includes N. Atlantic earthquake.

Seis. 19028 HNME 16,000 points beginning 0600 15 March 1969 noise.

Seis. 19029 HNME 16,000 points beginning 1337 15 March 1969 includes Aleutian earthquake.

Unclassified

Security Classification

DOCUMENT CONTROL DATA - R&D

(Security classification of title, body of abstract and indexing annotation must be entered when the overall report is classified)

1. ORIGINATING ACTIVITY (Corporate author)
TELEDYNE INDUSTRIES, INC.
ALEXANDRIA, VIRGINIA

2a. REPORT SECURITY CLASSIFICATION
Unclassified

2b GROUP

3. REPORT TITLE
ANALYSIS OF STRAIN SEISMOGRAPH DATA

4. DESCRIPTIVE NOTES (Type of report and inclusive dates)
Scientific

5. AUTHOR(S) (Last name, first name, initial)
Woolson, J.R.

6. REPORT DATE

7a. TOTAL NO. OF PAGES
62

7b. NO. OF REFS
12

8a. CONTRACT OR GRANT NO.
F33657-69-C-0913-PZ01

b. PROJECT NO.
VELA T/9706

ARPA Order No. 624

d. ARPA Program Code No. 9F10

9a. ORIGINATOR'S REPORT NUMBER(S)
250

9b. OTHER REPORT NO(S) (Any other numbers that may be assigned this report)

10. AVAILABILITY/LIMITATION NOTICES
This document is subject to special export controls and each transmittal to foreign governments or foreign nationals may be made only with prior approval of Chief, AFTAC.

11. SUPPLEMENTARY NOTES

12. SPONSORING MILITARY ACTIVITY
ADVANCED RESEARCH PROJECTS AGENCY
NUCLEAR MONITORING RESEARCH OFFICE
WASHINGTON, D.C.

13 ABSTRACT

Noise power on the short period pendulum and strain instruments has been compared at WMO and HNME. In the response band of the short period instruments, there are approximately four decades of relative power at HNME, and two decades at WMO. In one case analyzed the noise power at HNME is about 2½ times the noise power at WMO at 1 Hz.

Coherence was estimated as a measure of the existence of a linear transfer function between the vertical strain and the vertical pendulum. At HNME there exists a well-defined linear transfer function in the band 0.1 to 0.6 Hz. The low coherence at higher frequencies at HNME and throughout the 0.1 to 3.0 Hz band at WMO rule out the possibility of a linear transfer function between the vertical strain and vertical pendulum.

Multiple coherence, and rotation of the horizontal short period seismograms were used to infer the existence of unidirectional noise components. At HNME about 80 percent of the noise power is unidirectional in the 0.3 to 0.4 Hz band. At WMO the noise field has no apparent single preferred direction. Preliminary work on rotation of the horizontal strain instruments at WMO is presented. The technique uses a third horizontal instrument to establish the shear component of strain.

Examples of detailed analysis to establish wavetype using the vertical strain, together with the vertical pendulum and horizontal pendulum instruments are included.

14. KEY WORDS
Strain
Seismograph Data

Unclassified

Security Classification